Chin. Ann. Math.
30B(6), 2009, 653–682
DOI: 10.1007/s11401-009-0219-x

Chinese Annals of Mathematics, Series B

Coarse-Grained Langevin Approximations and Spatiotemporal Acceleration for Kinetic Monte Carlo Simulations of Diffusion of Interacting Particles****

Sasanka ARE* Markos A. KATSOULAKIS** Anders SZEPESSY***

(*Dedicated to Professor Andrew Majda on the Occasion of his* 60*th Birthday*)

Abstract Kinetic Monte Carlo methods provide a powerful computational tool for the simulation of microscopic processes such as the diffusion of interacting particles on a surface, at a detailed atomistic level. However such algorithms are typically computationally expensive and are restricted to fairly small spatiotemporal scales. One approach towards overcoming this problem was the development of coarse-grained Monte Carlo algorithms. In recent literature, these methods were shown to be capable of efficiently describing much larger length scales while still incorporating information on microscopic interactions and fluctuations. In this paper, a coarse-grained Langevin system of stochastic differential equations as approximations of diffusion of interacting particles is derived, based on these earlier coarse-grained models. The authors demonstrate the asymptotic equivalence of transient and long time behavior of the Langevin approximation and the underlying microscopic process, using asymptotics methods such as large deviations for interacting particles systems, and furthermore, present corresponding numerical simulations, comparing statistical quantities like mean paths, auto correlations and power spectra of the microscopic and the approximating Langevin processes. Finally, it is shown that the Langevin approximations presented here are much more computationally efficient than conventional Kinetic Monte Carlo methods, since in addition to the reduction in the number of spatial degrees of freedom in coarse-grained Monte Carlo methods, the Langevin system of stochastic differential equations allows for multiple particle moves in a single timestep.

Keywords Kinetic Monte Carlo methods, Diffusion, Fluctuations
2000 MR Subject Classification 82B24, 82B26, 82B80

1 Introduction

Stochastic interacting particle systems, such as the Ising model, have been adapted and

Manuscript received June 22, 2009. Published online September 25, 2009.
*Department of Mathematics and Statistics, University of Massachusetts, Amherst, MA 01003–9305, USA. E-mail: are@math.umass.edu
**Department of Mathematics and Statistics, University of Massachusetts, Amherst, MA 01003–9305, USA; Department of Applied Mathematics, University of Crete and Foundation of Research and Technology-Hellas, Heraklion 71405, Greece. E-mail: markos@math.umass.edu markos@tem.uoc.gr
***Matematiska Institutionen, Kungliga Tekniska Högskolan (Royal Institute of Technology), SE-100 44 Stockholm, Sweden. E-mail: szepessy@nada.kth.se
****Project supported by the National Science Foundation (Nos. DMS-0413864, DMS-0715125, DMS-0715125), the CDI-Type II Award (No. NSF-CMMI-0835673), the European Commision Marie-Curie Grant (No. FP6-517911) and the Swedish Research Council.

used to study a variety of problems in fields ranging from materials, chemical and biological sciences to image processing (see [2, 26]). Microscopic simulation methods such as molecular dynamics and Kinetic Monte Carlo (KMC) algorithms provide computational tools to simulate these stochastic models, but are restricted in terms of computational costs when attempting to simulate spatiotemporal scales observed in experiments. One method towards overcoming this problem was the development of coarse-grained Monte Carlo algorithms by A. J. Majda, D. G. Vlachos and one of the authors in [18, 23]. In recent literature, these methods were shown to be capable of efficiently describing much larger length scales than conventional Kinetic Monte Carlo simulations, while still incorporating information on microscopic interactions and fluctuations.

In particular, in [18, 23] a coarse-grained stochastic jump process with a reduced number of degrees of freedom was derived through local spatial averaging, approximating spin-flip and spin-exchange stochastic lattice dynamics of both Metropolis and Arrhenius types; furthermore the authors demonstrated the computational efficiency of the associated Coarse-Grained Monte Carlo (CGMC) simulations, and their ability to capture large scale morphologies. In [19, 22], rigorous analysis of CGMC algorithms as approximations of KMC algorithms in non-equilibrium is performed by estimating the error between the microscopic and the coarse-grained processes for spin flip lattice dynamics. Although coarse-graining methods provide a powerful computational tool in molecular simulations, it has been also observed that in some regimes important macroscopic properties may not be captured properly (see [1, 29]). For example, in CGMC simulations for lattice systems, hysteresis and critical behavior are not captured accurately for short and intermediate range potentials, while CGMC performs well in the case of long-range interactions (see [18, 20]). In [20] a coarse-graining strategy based on cluster expansions is developed, enabling higher order coarse-graining schemes for which the error is substantially reduced for short and intermediate range potentials. The higher order coarse-graining schemes are essentially derived by including multi-body interaction terms, while their key role in computing accurately dynamic properties in phase transition regimes, like mean times for domain switching, is discussed in detail in [3].

Based on these earlier coarse-grained models, in this paper we derive a coarse-grained Langevin system of stochastic differential equations (SDE) as an approximation of KMC diffusion of interacting particles. The primary motivation for deriving a coarse-grained SDE approximation, is that it will be much more computationally efficient than conventional Kinetic Monte Carlo methods, as well as CGMC: on one hand, we will have a reduction in the number of spatial degrees of freedom similarly to CGMC methods, while on the other, the Langevin system of stochastic differential equations will allow for multiple particle moves in a single timestep, giving rise to a significant spatiotemporal acceleration of the underlying KMC dynamics. We note here that in CGMC simulations only one particle moves per timestep, hence the Coarse-Grained Langevin (CGL) approximation developed here can be orders of magnitude faster than CGMC.

This perspective of Langevin approximations for jump processes has been studied extensively in several different contexts (see [5, 11, 12, 14, 21]). For instance, in [14] the authors studied the stochastic lattice systems with long range interactions modeling the adsorption/desorption

and surface diffusion mechanisms on a catalytic surface. In [14], the authors included random fluctuations in the mesoscopic mean field partial differential equations by a formal derivation of stochastic partial differential equations (SPDE) with space/time white noise; their approach relied on direct derivation from the microscopic Ising systems by means of a small noise, or equivalently large system-size, expansion in the corresponding high dimensional master equation. In [11] a Langevin SDE was derived based on the Kramers-Moyal expansion (see for instance [9]) of the chemical master equation for describing the chemical reactions in a well-stirred mixture of molecular species. Similarly, in [5], SPDE were derived, by using the expansion of the master equations, to study epitaxial growth in lattice models with random deposition of particles and surface diffusion.

In [21], the authors derived a system of coarse-grained system of SDE, approximating KMC algorithms for spin-flip dynamics. One of the new elements in [21] is the error estimates in weak topology, up to any bounded time, that identify the kind of expected values that can be accurately computed by employing the Langevin SDE approximation, within a given tolerance. Although such analysis shows rigorously that the derived SDE approximation is a controlled approximation of the KMC in finite time intervals, the long time behavior is not in agreement with the microscopic theory since the invariant measure of the SDE approximation is in principle different from the invariant measure for the master equation in regimes that exhibit bistability and phase transitions. In fact this was first observed in [12] where the authors studied the Langevin SDE approximation of a well-mixed birth-death process exhibiting bistability; the birth-death process considered in this paper is similar to the coarse-grained spin flip process with uniform interactions in [21]. Furthermore, in [12], it is shown by direct calculation in a 1D example, that the Langevin SDE approximation and the original jump birth-death process have different mean transition times between the two stable states. Such transitions are typically rare events, occurring at long times which scale with the size of the system, hence they are not captured by the error analysis in [21]. By contrast, in the present work we show that the derived Langevin SDE approximations for spin-exchange, diffusion dynamics indeed capture rare events and long time dynamics.

In this paper we derive a Coarse-Grained Langevin (CGL) system of stochastic differential equations as an approximation of the diffusion mechanism in many-body interacting particle systems. The approximating system of SDE has a reduced number of degrees of freedom, building on ideas from our earlier work [21], and our derivations are based on the CGMC jump process approximations of KMC diffusion already developed and tested in [23]. In contrast to the spin flip case discussed above, here we demonstrate the asymptotic equivalence of transient and long time behavior of the Langevin approximation and the underlying microscopic process, using asymptotics methods such as large deviations for interacting particles systems. More precisely, we obtain a time dependent action functional for the Langevin approximation and show that, asymptotically it is equivalent to the action functional of the mesoscopic limit of the microscopic diffusion process with interactions, where the latter was studied in [4]. This asymptotic equivalence of the action functionals shows that two processes, the microscopic and the CGL approximation, have the same asymptotic invariant measure and the same rare events.

Furthermore, we present corresponding numerical simulations, for the study of the transient and long time behavior of the Coarse-Grained Langevin SDE and the approximated microscopic process by comparing statistical quantities like mean paths, auto correlations and power spectra of the microscopic and the approximating Langevin processes. The numerical experiments are conducted using both CGMC and CGL. We compare the results from the two processes and also we compare them to the mesoscopic, local mean field solutions.

The paper is organized as follows. In Section 2 we present the microscopic and the coarse-grained model for the spin exchange mechanism. In Section 3, we derive the Coarse-Grained Langevin approximation of the diffusion mechanisms with interactions. In Section 4, we study the asymptotics and the large deviations of the CGL model. In Section 5 we present simulations using the CGL model for different boundary conditions and different regimes. We also study statistical properties, like auto correlation, to show that the noise in the CGL model is an accurate representation of the microscopic noise. In Appendix A we present a Langevin approximation of the spin flip mechanism and study its long time behavior using the example of the Curie-Weiss model.

2 Stochastic Interacting Particle Systems

In this section we present the background microscopic dynamics and the coarse-grained dynamics for spin exchange dynamics (see [18, 23]). The spin exchange dynamics have been successfully used to model diffusion mechanisms with interactions in numerous applications to study epitaxial growth, chemical kinetics and traffic flow (see [23, 30–32]).

2.1 Microscopic dynamics

We consider a microscopic stochastic model defined on a periodic lattice of size N which we denote by $\mathcal{L}_N = \{1, 2, \cdots, N\}$. All derivations are valid in higher dimensions, however for notational simplicity we restrict our presentation to the one-dimensional case. At each lattice site $x \in \mathcal{L}_N$ is an associated spin taking values 0 or 1. A spin configuration σ is an element of the configuration space $\Sigma = \{0,1\}^{\mathcal{L}_N}$ and we write $\sigma = \{\sigma(x) : x \in \mathcal{L}_N\}$ denoting by $\sigma(x)$ the spin at x.

The dynamics of Ising-type models considered in the literature consists of a sequence of spin flips and/or spin exchanges that correspond to different physical processes. A spin exchange between two neighboring sites $x, y \in \mathcal{L}_N$ is an exchange of the spins at the two locations. Physically these mechanisms describe the diffusion of particles on the lattice. The resulting stochastic process $\{\sigma_t\}_{t\geq 0}$ is a continuous time jump Markov process on $L^\infty(\Sigma;\mathbb{R})$ with generator

$$Lf(\sigma) = \sum_{x,y\in\mathcal{L}_N} c(x,y,\sigma)(f(\sigma^{(x,y)}) - f(\sigma))$$

for any test function $f \in L^\infty(\Sigma;\mathbb{R})$ (see [24]). Here $c(x,y,\sigma)$ denotes the rate of the process and $\sigma^{(x,y)}$ is the new configuration after a spin exchange between sites x and y. The microscopic Hamiltonian is given by

$$H(\sigma) = -\frac{1}{2}\sum_{x\in\mathcal{L}_N}\sum_{y\neq x} J(x-y)\sigma(x)\sigma(y) + \sum_{x\in\mathcal{L}_N} h(x)\sigma(x), \tag{2.1}$$

where the two-body inter-particle potential J describes the interaction between individual spins and h denotes the external field.

The spin exchange rates depend on the type of dynamics used, the simplest being the Metropolis-type dynamics. Here we implement spin exchange using Arrhenius-type dynamics. In this type of dynamics, which are widely used in KMC simulations, the particle overcomes an energy barrier in jumping from one site to another (see [18]). The Arrhenius spin exchange (surface diffusion) rate for the nearest neighbors x and y is given by

$$c(x,y,\sigma) = (1-\sigma(x))\sigma(y)c_0\mathrm{e}^{-\beta(U_0+U(x,\sigma))} + \sigma(x)(1-\sigma(y))c_0\mathrm{e}^{-\beta(U_0+U(y,\sigma))},$$

where

$$U(x,\sigma) = \sum_{\substack{y\in\mathcal{L}\\ y\neq x}} J(x-y)\sigma(y) - h(x), \tag{2.2}$$

where $h(x)$ denotes the external field at the site x and U_0 is the prefactor in the Arrhenius diffusion. The two-body interparticle potential J accounts for interactions between individual spins. The interaction potentials we consider are symmetric functions defined on the lattice $\mathcal{L}_N$ with a finite range interaction radius L. In this case each site interacts with $2L$ neighboring sites on the lattice $\mathcal{L}_N$ (note that the actual potential radius on lattice is $\frac{L}{N}$). We define the potential as

$$J(x-y) = \frac{1}{L}V\Big(\frac{x-y}{L}\Big),$$

where

$$V(r) = V(-r) = \begin{cases} V(|r|), & |r|\leq 1,\\ 0, & |r|>1. \end{cases}$$

For more general interactions like potentials with power decay or potentials with integrable singularity or potentials which have both repulsive and attractive interactions, we refer to [3].

2.2 Coarse-grained spin exchange dynamics

It is well-known that the microscopic dynamics are computationally very demanding, especially in the spin-exchange case, due to the detailed nature of the local conservation law imposed by the dynamics that slow down the evolution of macroscopic morphologies. The coarse-graining techniques, at least for systems with long range interactions, offer a computationally efficient alternative while being able to capture the large scale structures and reduce the order of the system. It should be noted that, in the case of spin-exchange dynamics, coarse-graining in space also induces a coarse-graining of the microscopic process in time. In fact, when we coarse-grain by q points on the microscopic lattice, we also coarse-grain the microscopic time by q^2 (see [23]). This coarse-graining in time is demonstrated in Figures 6 and 7 in Section 5.

Using the above microscopic process on the lattice $\mathcal{L}_N$, we can derive a coarse-grained Markov process $\{\eta_t\}$ set on the coarse lattice $\mathcal{L}_m = \{1,2,\cdots,m\}$ (see [18]). Each coarse cell C_k consists of q (the level of coarse-graining) microscopic lattice points:

$$\eta_t(k) = \sum_{y\in C_k}\sigma_t(y), \quad k=1,\cdots,m.$$

The configuration space is $\mathcal{H}_{mq} = \{0, 1, \cdots, q\}^{\mathcal{L}_m}$, where $\eta_t = \{\eta(k) : k \in \mathcal{L}_m\}$ and $\eta(k) \in \{0, 1, \cdots, q\}$ is the coverage of the coarse cell C_k. We define the approximation $\overline{U}(k, \eta)$ of the potential $U(x, \sigma)$, (2.2), at the coarse level (for more details see [18, 23]),

$$\overline{U}(k, \eta) = \sum_{\substack{l \in \mathcal{L}_m \\ l \neq k}} \overline{J}(k, l)\eta(l) + \overline{J}(0, 0)(\eta(k) - 1) - \overline{h}(k). \tag{2.3}$$

For any $x \in C_k$, we have

$$U(x, \sigma) = \overline{U}(k, \eta) + O\Big(\frac{q}{L}\Big).$$

The error estimate above gives us an indication of when the coarse-graining is a good approximation of the microscopic process. A detailed quantification of such errors can be found in [3]. The coarse-grained interaction potential $\overline{J}$ is computed as the average of the pair-wise interactions between the microscopic spins between the coarse cells C_k and C_l,

$$\overline{J}(k, l) = \frac{1}{q^2} \sum_{\substack{x \in C_k \\ y \in C_l}} J(x - y) \qquad \text{for } k \neq l,$$

$$\overline{J}(0, 0) = \frac{1}{q(q-1)} \sum_{\substack{x, y \in C_k \\ y \neq x}} J(x - y) \quad \text{for } k = l.$$

The rate $\overline{c}(k \mapsto l, \eta)$ which describes the migration of a particle from the coarse cell C_k to C_l is given by

$$\overline{c}(k \mapsto l, \eta) = \overline{c}_{kl} = \frac{c_0}{q}\eta(k)(q - \eta(l)) \exp[-\beta(U_0 + \overline{U}(k, \eta))] \tag{2.4}$$

if k, l are nearest neighbors and $\overline{c}(k \mapsto l, \eta) = 0$ otherwise. These rates are formally derived from the microscopic process and under the assumption that the particles in each coarse cell C_k are at local equilibrium, i.e., we can replace $\sigma(x)$ with $q^{-1}\eta(k)$ (respectively $\sigma(y)$ with $q^{-1}\eta(l)$). This last substitution somewhat parallels the "Replacement Lemma" (see [24]) in the derivation of deterministic hydrodynamic limits for interacting particle systems. Hence for any $g \in L^\infty(\mathcal{H}_{mq}; \mathbb{R})$ the new coarse-grained Markov process on $\mathcal{H}_{mq}$ satisfies

$$\frac{\mathrm{d}}{\mathrm{d}t} Eg(\eta) = M_c g(\eta) = E \sum_{k, l \in \mathcal{L}_m} \overline{c}(k \mapsto l, \eta)(g(\eta + \delta_l - \delta_k) - g(\eta)), \tag{2.5}$$

where δ_l is a configuration such that $\delta_l(k) = 0$, $k \neq l$ and $\delta_l(l) = 1$. Now using the generator given by (2.5) we define a new Markov process $\{\overline{\eta}_t\}$ on the coarse lattice $\mathcal{L}_m$, that corresponds to the local average coverage

$$\overline{\eta}(k) = \frac{1}{q}\eta(k), \quad k = 1, \cdots, m$$

with configuration space $\overline{\mathcal{H}}_{mq} = \{0, \frac{1}{q}, \cdots, 1\}^{\mathcal{L}_m}$. For any $\overline{g} \in L^\infty(\overline{\mathcal{H}}_{mq}; \mathbb{R})$, this process satisfies

$$\frac{\mathrm{d}}{\mathrm{d}t} E[\overline{g}(\overline{\eta})] = M_c[\overline{g}(\overline{\eta})] = E \sum_{k, l \in \mathcal{L}_m} \overline{c}(k \mapsto l, \overline{\eta})\Big(\overline{g}\Big(\overline{\eta} + \frac{1}{q}(\delta_l - \delta_k)\Big) - \overline{g}(\overline{\eta})\Big). \tag{2.6}$$

In [20], detailed error analysis at equilibrium was presented to quantify the effectiveness of the above coarse-graining scheme and along with higher-order coarse-graining scheme. All the error estimates are calculated in terms of the specific relative entropy of the equilibrium Gibbs measures, using the concept of relative entropy as a quantitative measure for the loss of information during coarse-graining the finer (microscopic) scales.

3 Langevin SDE Approximation of Coarse-Grained Markov Process

Even though CGMC simulations are computationally more efficient than the MC simulations, they are also known to be computationally expensive, especially in phase transition regimes. Langevin approximations are computationally faster the MC/CGMC simulations because in the Langevin approximation more than one particles can be moved in one timestep where as in MC simulations only one particle moves per timestep. The focus of this work is to approximate the coarse-grained Markov process $\{\overline{\eta}_k\}$ by $\{\widetilde{\eta}_k\}$ set on the coarse lattice $\mathcal{L}_m = \{1, 2, \cdots, m\}$, where $\{\widetilde{\eta}_k\}$ is the solution of the system of stochastic differential equations (CGL) given by

$$\mathrm{d}\widetilde{\eta} = a(\widetilde{\eta})\mathrm{d}t + b(\widetilde{\eta})\mathrm{d}B_t, \tag{3.1}$$

where $\widetilde{\eta} = \{\widetilde{\eta}_k : k \in \mathcal{L}_m\}$ set on the configuration space $\widetilde{\mathcal{H}}_{mq} = [0,1]^{\mathcal{L}_m}$, $a(\widetilde{\eta}) = \{a(k, \widetilde{\eta}) : k \in \mathcal{L}_m\}$ and $b(\widetilde{\eta}) = (b_{ij}(\widetilde{\eta}))$, $1 \le i, j \le m$.

The generator of this process is defined on an arbitrary observable $\widetilde{g} \in L^\infty(\widetilde{\mathcal{H}}_{mq}; \mathbb{R})$ as

$$\frac{\mathrm{d}}{\mathrm{d}t}[E\widetilde{g}(\overline{\eta})] = \sum_{k\in\mathcal{L}_m} a(k, \widetilde{\eta})\frac{\partial \widetilde{g}}{\partial x_k} + \frac{1}{2}\sum_{k,l\in\mathcal{L}_m} (bb^{\mathrm{T}})_{kl}\frac{\partial^2 \widetilde{g}}{\partial x_k \partial x_l}. \tag{3.2}$$

Now for any $g \in L^\infty(\overline{\mathcal{H}}_{mq}; \mathbb{R}) \subset L^\infty(\widetilde{\mathcal{H}}_{mq}; \mathbb{R})$, we can estimate the error $E[g(\overline{\eta}_T)] - E[g(\widetilde{\eta}_T)]$, using (2.6), (3.2) and a slight abuse of notation,

$$\begin{aligned} E[g(\overline{\eta}_T)] - E[g(\widetilde{\eta}_T)] = E\int_0^T \mathrm{d}t\Big[&\sum_{k,l\in\mathcal{L}_m} \overline{c}(k \mapsto l, \overline{\eta})\Big(u\Big(\overline{\eta}_t + \frac{1}{q}(\delta_l - \delta_k), t\Big) - u(\overline{\eta}_t, t)\Big) \\ &- \sum_{k\in\mathcal{L}_m} a(k)\frac{\partial u}{\partial x_k}(\overline{\eta}_t, t) - \frac{1}{2}\sum_{k,l\in\mathcal{L}_m} (bb^{\mathrm{T}})_{kl}\frac{\partial^2 u}{\partial x_k \partial x_l}(\overline{\eta}_t, t)\Big], \end{aligned} \tag{3.3}$$

where similarly to [21] we set

$$u(y, t) = E[g(\widetilde{\eta}_T)|\widetilde{\eta}_t = y],$$

$a(k) = a(k; \widetilde{\eta})$ and $(bb^{\mathrm{T}})_{kl} = (bb^{\mathrm{T}})_{kl}(\widetilde{\eta})$. Using a Taylor series expansion of the first term in the above integrand (i.e., the generator of the coarse-grained Markov process given by (2.6)), we get

$$\begin{aligned} E[g(\overline{\eta}_T)] - E[g(\widetilde{\eta}_T)] = E\int_0^T \Big[&\sum_{k\in\mathcal{L}_m} \Big(\frac{1}{q}(\overline{c}_{k(k+1)} + \overline{c}_{k(k-1)} - \overline{c}_{(k+1)k} - \overline{c}_{(k-1)k})\frac{\partial u}{\partial x_k}(\overline{\eta}_t, t) \\ &- \frac{1}{2q^2}(\overline{c}_{k(k-1)} + \overline{c}_{(k-1)k})\frac{\partial^2 u}{\partial x_k \partial x_{k-1}}(\overline{\eta}_t, t) \\ &+ \frac{1}{2q^2}(\overline{c}_{k(k+1)} + \overline{c}_{k(k-1)} + \overline{c}_{(k+1)k} + \overline{c}_{(k-1)k})\frac{\partial^2 u}{\partial^2 x_k}(\overline{\eta}_t, t) \\ &- \frac{1}{2q^2}(\overline{c}_{k(k+1)} + \overline{c}_{(k+1)k})\frac{\partial^2 u}{\partial x_k \partial x_{k+1}}(\overline{\eta}_t, t)\Big) \\ &- \sum_{k\in\mathcal{L}_m} a(k)\frac{\partial u}{\partial x_k}(\overline{\eta}_t, t) - \frac{1}{2}\sum_{k,l\in\mathcal{L}_m} (bb^{\mathrm{T}})_{kl}\frac{\partial^2 u}{\partial x_k \partial x_l}(\overline{\eta}_t, t)\Big]\mathrm{d}t \\ &+ O\Big(\frac{1}{q^3}\Big), \end{aligned} \tag{3.4}$$

where we denote $c_{kl} = \overline{c}(k \mapsto l, \overline{\eta})$. The error term (3.4) is due to the Taylor expansion and its effects are highlighted in the simulations presented in Section 5 (see Figure 3).

We can now turn our attention to the selection of the drift and diffusion matrix in (3.1), based on minimizing the error on the right hand side of (3.4). The optimal drift for minimal error is given by the first order term of the expansion

$$a(k) = \frac{1}{q}(\overline{c}_{(k+1)k} + \overline{c}_{(k-1)k} - \overline{c}_{k(k+1)} - \overline{c}_{k(k-1)}), \tag{3.5}$$

where $\overline{c}_{kl}$ is defined in (2.4). The second order terms in (3.3) give the optimal diffusion matrix $D = bb^{\mathrm{T}}$. It can be seen that D is a symmetric tridiagonal matrix given by

$$\begin{aligned} D_{kk} &= \frac{1}{q^2}(\overline{c}(k \mapsto k+1, \eta) + \overline{c}(k+1 \mapsto k, \eta) + \overline{c}(k \mapsto k-1, \eta) + \overline{c}(k-1 \mapsto k, \eta)), \\ D_{k(k+1)} &= -\frac{1}{q^2}(\overline{c}(k \mapsto k+1, \eta) + \overline{c}(k+1 \mapsto k, \eta)), \\ D_{k(k-1)} &= -\frac{1}{q^2}(\overline{c}(k \mapsto k-1, \eta) + \overline{c}(k-1 \mapsto k, \eta)), \\ D_{kl} &= 0, \quad \text{if } |k-l| \geq 2. \end{aligned} \tag{3.6}$$

This in turn gives that the matrix b is as follows:

$$\begin{aligned} b_{kk} &= \sqrt{-D_{k(k+1)}} = \frac{1}{q}\sqrt{\overline{c}(k \mapsto k+1, \eta) + \overline{c}(k+1 \mapsto k, \eta)}\,, \\ b_{(k+1)k} &= -b_{kk}, \\ b_{ij} &= 0, \quad \text{otherwise.} \end{aligned} \tag{3.7}$$

Boundary conditions define the rates at the two boundary cells which in turn determine the coefficients of the drift vector (3.5) and diffusion matrix (3.7). The two boundary conditions we discuss in this paper are periodic and Dirichlet and the detailed calculations involving them are included in Appendix B.

Finally we remark on error when using CGL in order to approximate conventional KMC diffusion. We can write the error from the Langevin approximation as the error from coarse-graining which is dependent on the coarse-graining parameters and error from the Taylor expansions in (3.4). Hence the total error for the Langevin approximation of the coarse-grained Markov process when compared to the microscopic process is formally given by

$$\text{total error} \simeq O\Big(\frac{q}{L}\Big) + O\Big(\frac{1}{q^3}\Big). \tag{3.8}$$

4 Asymptotics, Large Deviations and Connections to SPDE

Langevin approximations even though computationally attractive are often handicapped in terms of their long time behavior. This was first observed in [12], where it was shown that exit times of a Langevin approximation derived using a small parameter expansion of the Fokker-Planck equation are different from the exit times of the approximated bistable birth-death jump process. The principal challenge in this section is to show that the Langevin approximation

of diffusion mechanisms presented in Section 3 does not suffer from such shortcomings and is an accurate approximation of the underlying microscopic process and corresponding KMC algorithms for both transient and long-time regimes.

In this direction, we first formally validate the Langevin approximation presented in this paper by demonstrating that the CGL model asymptotically shares the long time mesoscopic behavior given by (4.1), the stochastic Langevin PDE derived as a zero lattice-size approximation from microscopic Arrhenius dynamics (see [31]). This discussion is formal in nature because with the present SPDE theory it is difficult to formulate proper weak solutions for non-linear models like the Cahn-Hilliard-Cook (CHC) type models. In the second part of this section we study long time behavior and show that it is identical to the microscopic process by deriving a time dependent action functional which is similar to the action functional derived in [4] where the authors derive a large deviation principle from the hydrodynamic limit of an exclusion particle system with long range interactions. The equivalence of the rate of functionals suggests that the CGL gives rise to the same transition rates and rare events as the original microscopic system and corresponding KMC algorithm. This latter argument can also be viewed as an indirect but mathematically rigorous way of showing the connection of CGL with the CHC models (see Section 3).

4.1 Connections to Cahn-Hilliard-Cook-type SPDE

In [23, 31] the authors highlighted the connection of the coarse-grained diffusion dynamics to stochastic mesoscopic equations and Cahn-Hilliard-Cook-type (CHC) SPDE given by

$$\begin{aligned}\rho_t =& \partial_x\{T_0 \exp[-\beta J * \rho](\partial_x \rho - \beta\rho(1-\rho)\partial_x J * \rho)\} \\ &+ \frac{1}{\sqrt{N}}\partial_x \cdot \{[2T_0 \exp[-\beta J * \rho]\rho(1-\rho)]^{\frac{1}{2}}\dot{W}\},\end{aligned} \tag{4.1}$$

where N is the size of the microscopic system, $T_0 = \exp[-\beta U_0]$, and $\dot{W}$ is space time white noise. The weak formulation of (4.1) for any test function ϕ is given by

$$\begin{aligned}\langle \phi, \rho_t\rangle =& \langle \partial_x\phi, T_0 \exp[-\beta J * \rho](\partial_x\rho - \beta\rho(1-\rho)\partial_x J * \rho)\rangle \\ &+ \frac{1}{\sqrt{N}}\langle \partial_x\phi, [2T_0\rho(x)(1-\rho(x))\exp[-\beta J * \rho(x)]]^{\frac{1}{2}}\dot{W}\rangle.\end{aligned} \tag{4.2}$$

In a similar mesoscopic theory presented earlier (see [10]), the authors derive an equation similar to (4.1) for the case of Metropolis dynamics:

$$\rho_t = T_0\partial_x\{\partial_x\rho - \beta\rho(1-\rho)\partial_x J * \rho\} + \frac{1}{\sqrt{N}}\partial_x \cdot \{(2T_0\rho(1-\rho))^{\frac{1}{2}}\dot{W}\}. \tag{4.3}$$

In this subsection we first show formally that the CGL derived in Section 3, by focusing on the deterministic drift term and the stochastic noise term separately, behaves like the SPDE given (4.1) in the zero lattice-size limit. This discussion is formal in the sense that it does not directly derive (4.1) but provides an insight into the asymptotics of the system; some of the calculations used in this discussion are related to the results in the next subsection. For the

sake of simplicity in notation, we carry out all calculations in one space dimension, although all calculations trivially extend to any dimension.

If we assume that $\widetilde{\eta}_t(k)$ in the zero lattice-size limit evolves slowly, i.e., behaves like a density $\rho(\frac{k}{m},t)$, then we show that in the limit $\rho(x,m^2t)$ solves the SPDE in (4.1) using a straightforward Taylor series expansion in the small parameter $\frac{1}{m}$ of the drift and diffusion coefficients, expanding the transition rates defined in (2.4):

$$\begin{aligned}
c(k\mapsto k+1,\widetilde{\eta}) &= q\rho(x_k)(1-\rho(x_{k+1}))\exp[-\beta(U_0+\overline{U}(k,\rho))]\\
&= q\rho(x_k)\Big(1-\rho(x_k)-\frac{1}{m}\partial_x\rho(x_k)\Big)\exp[-\beta(U_0+\overline{U}(k,\rho))]+O\Big(\frac{1}{m^2}\Big)\\
&= q\rho(x_k)(1-\rho(x_k))\exp[-\beta(U_0+\overline{U}(k,\rho))]\\
&\quad - q\rho(x_k)\frac{1}{m}\partial_x\rho(x_k)\exp[-\beta(U_0+\overline{U}(k,\rho))]+O\Big(\frac{1}{m^2}\Big),\\
c(k+1\mapsto k,\widetilde{\eta}) &= q\rho(x_{k+1})(1-\rho(x_k))\exp[-\beta(U_0+\overline{U}(k+1,\rho))]\\
&= q\rho(x_k)(1-\rho(x_k))\exp[-\beta(U_0+\overline{U}(k,\rho))]\\
&\quad - q\rho(x_k)(1-\rho(x_k))\exp[-\beta(U_0+\overline{U}(k,\rho))]\frac{\beta}{m}\partial_x\overline{U}(k,\rho)\\
&\quad + q(1-\rho(x_k))\frac{1}{m}\partial_x\rho(x_k)\exp[-\beta(U_0+\overline{U}(k,\rho))]+O\Big(\frac{1}{m^2}\Big),
\end{aligned}\tag{4.4}$$

where $\rho(x_k)$ denotes the slowly varying field $\rho(\frac{k}{m})\approx\widetilde{\eta}(k)$.

Using the above expansions, we rewrite the drift in (3.5) and the diffusion coefficients in (3.6) as

$$\begin{aligned}
a(k) &= \frac{1}{m}\rho(x_k)(1-\rho(x_k))\partial_x\exp[-\beta(U_0+\overline{U}(k,\rho))]\\
&\quad + \frac{1}{m}\partial_x\rho(x_k)\exp[-\beta(U_0+\overline{U}(k,\rho))]\\
&\quad - \frac{1}{m}\rho(x_{k-1})(1-\rho(x_{k-1}))\partial_x\exp[-\beta(U_0+\overline{U}(k-1,\rho))]\\
&\quad - \frac{1}{m}\partial_x\rho(x_{k-1})\exp[-\beta(U_0+\overline{U}(k-1,\rho))]+O\Big(\frac{1}{m^2}\Big),\\
D_{k(k+1)} &= \frac{2}{q}\rho(x_k)(1-\rho(x_k))\exp[-\beta(U_0+\overline{U}(k,\rho))]\\
&\quad + \frac{1}{mq}\partial_x\{\rho(x_k)(1-\rho(x_k))\exp[-\beta(U_0+\overline{U}(k,\rho))]\}+O\Big(\frac{1}{m^2}\Big),\\
D_{k(k-1)} &= \frac{2}{q}\rho(x_k)(1-\rho(x_k))\exp[-\beta(U_0+\overline{U}(k,\rho))]\\
&\quad - \frac{1}{mq}\partial_x\{\rho(x_k)(1-\rho(x_k))\exp[-\beta(U_0+\overline{U}(k,\rho))]\}+O\Big(\frac{1}{m^2}\Big).
\end{aligned}\tag{4.5}$$

Also note that

$$D_{kk}=-(D_{k(k-1)}+D_{k(k+1)}).$$

For any test function ϕ, we define

$$\langle\phi,\rho\rangle_{l^2}=\frac{1}{m}\sum_{k\in\mathcal{L}_m}\rho(x_k)\phi(x_k),\quad\text{where } x_k=\frac{k}{m}.$$

Using the above calculations we seek to recover (4.2) from (3.1):

$$\begin{aligned}\frac{\mathrm{d}}{\mathrm{d}t}\langle\phi,\rho\rangle_{l^2} &= \frac{1}{m}\sum_{k\in\mathcal{L}_m}\frac{\mathrm{d}\rho(k,t)}{\mathrm{d}t}\phi(x_k)\\ &= \frac{1}{m}\sum_{k\in\mathcal{L}_m}\Big(a_k(\rho)+\sum_{j\in\mathcal{L}_m}b_{kj}(\rho)\frac{\mathrm{d}B_j}{\mathrm{d}t}\Big)\phi(x_k)\\ &= \frac{1}{m}\sum_{k\in\mathcal{L}_m}a_k(\rho)\phi(x_k)+\frac{1}{m}\sum_{k\in\mathcal{L}_m}\Big(\sum_{j\in\mathcal{L}_m}b_{kj}(\rho)\frac{\mathrm{d}B_j}{\mathrm{d}t}\Big)\phi(x_k)\\ &= \frac{1}{m}\sum_{k\in\mathcal{L}_m}a_k(\rho)\phi(x_k)+\frac{1}{m}\sum_{k\in\mathcal{L}_m}\Big(\sum_{j\in\mathcal{L}_m}b_{jk}(\rho)\phi(x_j)\Big)\frac{\mathrm{d}B_k}{\mathrm{d}t}\\ &= \underbrace{\frac{1}{m}\sum_{k\in\mathcal{L}_m}a_k(\rho)\phi(x_k)}_{\text{drift term}}+\underbrace{\frac{1}{m}\sum_{k\in\mathcal{L}_m}\Big(\sum_{j\in\mathcal{L}_m}b^{\mathrm{T}}_{kj}(\rho)\phi(x_j)\Big)\frac{\mathrm{d}B_k}{\mathrm{d}t}}_{\text{stochastic term}}.\end{aligned}\tag{4.6}$$

The drift term in (4.6) can be written as (see Appendix A)

$$\frac{1}{m}\sum_k a_k(\rho)\phi(x_k)=\frac{1}{m^2}\langle\partial_x\{T_0\exp[-\beta J*\rho](\partial_x\rho-\beta\rho(1-\rho)\partial_x J*\rho)\},\phi\rangle_{l^2}+O\Big(\frac{1}{m^3}\Big),\tag{4.7}$$

where $T_0=\exp[-\beta U_0]$ and $\overline{U}(k,\rho)=\sum_{\substack{l\in\mathcal{L}_m\\ l\neq k}}\overline{J}(k,l)\rho(l)+\overline{J}(0,0)(\rho(k)-1)-\overline{h}(k)$.

The covariance of the stochastic term in (4.6) evaluated at two different test functions ϕ_1, ϕ_2 is (see Appendix A)

$$\begin{aligned}&\Big\langle\sum_{k\in\mathcal{L}_m}\sum_{j\in\mathcal{L}_m}b^{\mathrm{T}}_{jk}(\rho)\phi_1(x_j)\frac{\mathrm{d}B_k}{\mathrm{d}t},\sum_{l\in\mathcal{L}_m}\sum_{i\in\mathcal{L}_m}b^{\mathrm{T}}_{il}(\rho)\phi_2(x_i)\frac{\mathrm{d}B_l}{\mathrm{d}t}\Big\rangle\\ &=\frac{1}{mq}\int_0^1 2T_0\rho(x)(1-\rho(x))\exp[-\beta J*\rho]\partial_x\phi_1(x)\partial_x\phi_2(x)\mathrm{d}x+O\Big(\frac{1}{m^2}\Big),\end{aligned}\tag{4.8}$$

where $T_0=\exp[-\beta U_0]$ and $\overline{U}(k,\rho)=\sum_{\substack{l\in\mathcal{L}_m\\ l\neq k}}\overline{J}(k,l)\rho(l)+\overline{J}(0,0)(\rho(k)-1)-\overline{h}(k)$.

Using similar calculations to those in (4.8) the covariance of the stochastic term in (4.1) evaluated at two different test function ϕ_1, ϕ_2 is (see Appendix A)

$$\begin{aligned}&\Big\langle\int\frac{1}{\sqrt{mq}}\partial_x\{[2T_0\exp[-\beta J*\rho]\rho(1-\rho)]^{\frac{1}{2}}\dot{W}\}\phi_1(x)\mathrm{d}x,\\ &\quad\int\frac{1}{\sqrt{mq}}\partial_x\{[2T_0\exp[-\beta J*\rho]\rho(1-\rho)]^{\frac{1}{2}}\dot{W}\}\phi_2(y)\mathrm{d}y\Big\rangle\\ &=\frac{1}{mq}\int\{2T_0\rho(x)(1-\rho(x))\exp[-\beta J*\rho(x)]\}\partial_x\phi_1(x)\partial_x\phi_2(x)\mathrm{d}x,\end{aligned}\tag{4.9}$$

where $T_0=\exp[-\beta U_0]$.

The factor $\frac{1}{m^2}$ in (4.7) suggests a time scaling noted also in CGMC methods in [23]. Indeed, after introducing the time rescaling

$$t\mapsto tm^2,\tag{4.10}$$

we will have exactly the discretized form of the drift term in (4.2). Regarding the covariance in (4.8) we first note that with the aforementioned rescaling, white noise scales as $\dot{W}_{m^2t}=\frac{1}{m}\dot{W}_t$;

furthermore, (4.8) corresponds exactly to the discretized form of the covariance obtained in (4.9) on the coarse lattice with size $\frac{1}{m}$, and from the scaling of the white noise and (4.6) we formally obtain that in the $m \to \infty$ limit the CGL model agrees with the CHC SPDE (4.2).

4.2 Rare events, large deviations and action functionals

As stated earlier the main goal of this subsection is to show that the Langevin approximation presented in this paper is an accurate approximation of the microscopic process for transient and long time regimes, including rare events and phase transitions. In order to do this, we show an asymptotic equivalence of the large deviations of the CGL's and the microscopic process as defined by their respective action functionals. In this subsection, we derive a time dependent large deviation rate for the CGL approximation presented in Section 3 in the form of an action functional. We show that the derived action functional is asymptotically identical to the action functional derived in [4]: there the authors derived a Large Deviations Principle (LDP) for a system with long range interactions that models diffusion of interacting particles. The results of the LDP type were first obtained in [25] in the context of the symmetric exclusion process and later extended in [4] for the case of Kawasaki dynamics with long range interactions. This derivation is also an indirect but rigorous way of establishing the connection of CGL to SPDE's hinted by the formal discussion in Subsection 4.1.

In order to derive the action functional for CGL, we recall some background from [7, 8] regarding the large deviations of stochastic differential equations. For every $0 < \varepsilon \ll 1$, let $(X_t^\varepsilon, P_x^\varepsilon)$ be a Markov process such that $X_t \in \mathbb{R}^k$, associated with the generator A^ε defined for a twice continuously differentiable test function $f = f(x)$ as

$$A^\varepsilon f(x) = \sum_i c_i(x)\frac{\partial f}{\partial x_i} + \frac{\varepsilon}{2}\sum_{i,j} d^{ij}(x)\frac{\partial^2 f}{\partial x_i \partial x_j}. \tag{4.11}$$

The rate function for the Markov process $(X_t^\varepsilon)_{t\geq 0}$ defined for any absolutely continuous function $\psi : [0,T] \mapsto \mathbb{R}^k$ is given by

$$S_{[0,T]}(\psi) = \int_0^T L(\psi, \psi_t)\mathrm{d}t, \tag{4.12}$$

where

$$L(x,\beta) = \sup_{\alpha\in\mathbb{R}^k}\Big\{\langle\alpha,\beta\rangle - \Big(\langle c(x),\alpha\rangle + \frac{1}{2}\langle\alpha, d(x)\alpha\rangle\Big)\Big\}.$$

For rigorous definitions and a detailed exposition of large deviations for diffusion processes, we refer to [7, 8]. Formally though, for $\delta, \varepsilon > 0$, we have the asymptotic formula

$$\mathbf{P}\{\mu(X^\varepsilon, \psi) \leq \delta\} \sim \exp\{-\varepsilon^{-1} S_{[0,T]}(\psi)\},$$

where μ is a metric in a suitably defined function space. Intuitively we can think of the function ψ as one of the probable paths of the Markov process $(X_t^\varepsilon)_{t\geq 0}$, μ as a measure of the distance between the two paths and the rate function $S_{[0,T]}(\psi)$ as the functional that assigns a probability to the event that X_t^ε follows the path ψ.

Next, we recover the action functional corresponding to the CGL approximate SDE derived in Section 3,

$$\mathrm{d}\widetilde{\eta} = a(\widetilde{\eta})\mathrm{d}t + b(\widetilde{\eta})\mathrm{d}B_t,$$

where $\widetilde{\eta} = \{\widetilde{\eta}_k : k \in \mathcal{L}_m\}$, $a(\widetilde{\eta})$ is defined in (3.5), and $b(\widetilde{\eta})$ is defined in (3.7). A direct application of (4.7) and (4.8) and the time rescaling (4.10) results in a generator scaling similar to (4.11) with a small parameter $\varepsilon = \frac{1}{m}$.

The corresponding action functional is obtained by using (4.7) and (4.8) in (4.12). For $\Psi : [0,T] \times [0,1] \mapsto \mathbb{R}$ and $G : [0,1] \mapsto \mathbb{R}$, we set

$$S_{0T}^m(\Psi) = \int_0^T L^m(\Psi, \Psi_t)\mathrm{d}t,$$

where

$$L^m(\Psi, \Psi_t) = \sup_G \Big\{ \langle g, \psi_t - m^2 a(\psi_t)\rangle_{l^2} - \frac{1}{2}\langle g, mN(bb^{\mathrm{T}})(\psi_t)g\rangle_{l^2} \Big\}, \tag{4.13}$$

$g = \{g_k = G(x_k) : x_k = \frac{k}{m}\} \in \mathbb{R}^m$, $\psi(t) = \{\Psi(t, x_k) : x_k = \frac{k}{m}\} \in \mathbb{R}^m$, and

$$\langle a, b\rangle_{l^2} = \frac{1}{m}\sum_{k\in\mathcal{L}_m} a(k)b(k), \quad \forall\, a, b \in \mathbb{R}^m.$$

Using the same approximations and calculations made in (4.7) and (4.8), we can show that the two terms inside the supremum in the definition of L^m as $m \to \infty$ behave as

$$\begin{aligned}
\langle g, \psi_t - m^2 a(\psi)\rangle_{l^2} &= \langle g, \psi_t\rangle_{l^2} - \langle g, m^2 a(\psi)\rangle_{l^2} \\
&= \langle G, \Psi_t\rangle_{l^2} - \langle G, T_0[\Psi_x \exp[-\beta\overline{U}\,] + \Psi(1-\Psi)[\exp[-\beta\overline{U}\,]]_x]_x\rangle_{l^2} \\
&\to \langle G, \Psi_t - T_0[\Psi_x \exp[-\beta\overline{U}\,] + \Psi(1-\Psi)[\exp[-\beta\overline{U}\,]]_x]_x\rangle_{L^2}, \\
\langle g, mN(bb^{\mathrm{T}})(\psi)g\rangle_{l^2} &\to T_0\langle G_x, [\Psi(1-\Psi)\exp[-\beta\overline{U}\,]]G_x\rangle_{L^2},
\end{aligned}$$

where $T_0 = \exp[-\beta U_0]$ and $\langle \zeta, \xi\rangle_{L^2} = \int_0^1 \zeta\xi\,\mathrm{d}x$.

So asymptotically as $m \to \infty$, the functional L defined in (4.13) is expected to converge to

$$\begin{aligned}
L(\Psi, \Psi_t) = \sup_G \Big\{ &\int_0^1 G(\Psi_t - T_0[\Psi_x \exp[-\beta\overline{U}] + \Psi(1-\Psi)[\exp[-\beta\overline{U}\,]]_x]_x)\mathrm{d}x \\
&- \int_0^1 T_0\Psi(1-\Psi)\exp[-\beta\overline{U}\,]G_x^2\mathrm{d}x \Big\}.
\end{aligned} \tag{4.14}$$

A rigorous proof of the above formal large derivation could be carried out by combining using Γ-convergence arguments and the arguments in [4].

In order to clarify the structure of the action functional, we rewrite (4.14) in terms of a function $H = H(x,t)$, which is the maximizer of (4.14). Then for any test function Φ, by definition we have

$$\begin{aligned}
0 = &\frac{\mathrm{d}}{\mathrm{d}\epsilon}\{\langle H + \epsilon\Phi, \Psi_t - T_0[\Psi_x \exp[-\beta\overline{U}\,] + \Psi(1-\Psi)[\exp[-\beta\overline{U}\,]]_x]_x\rangle_{L^2} \\
&- T_0\langle (H+\epsilon\Phi)_x, [\Psi(1-\Psi)\exp[-\beta\overline{U}\,]](H+\epsilon\Phi)_x\rangle_{L^2}\} \\
= &\langle \Phi, \Psi_t - T_0[\Psi_x \exp[-\beta\overline{U}\,] + \Psi(1-\Psi)[\exp[-\beta\overline{U}\,]]_x]_x\rangle_{L^2} \\
&- \langle \Phi_x, T_0\Psi(1-\Psi)\exp[-\beta\overline{U}\,]H_x\rangle_{L^2} - \langle H_x, T_0\Psi(1-\Psi)\exp[-\beta\overline{U}\,]\Phi_x\rangle_{L^2} \\
= &\langle \Phi, t\Psi_t - T_0[\Psi_x \exp[-\beta\overline{U}\,] + \Psi(1-\Psi)[\exp[-\beta\overline{U}\,]]_x]_x\rangle_{L^2} \\
&- 2\langle \Phi, [T_0\Psi(1-\Psi)\exp[-\beta\overline{U}\,]H_x]_x\rangle_{L^2}.
\end{aligned}$$

Hence we have that the maximizer $H = H(x,t)$ in (4.14) satisfies

$$\Psi_t = T_0[\Psi_x \exp[-\beta\overline{U}\,] + \Psi(1-\Psi)[\exp[-\beta\overline{U}\,]]_x + 2\Psi(1-\Psi)\exp[-\beta\overline{U}\,]H_x]_x,$$

which can be rewritten as the deterministic part of (4.1), where $H = H(x,t)$ acts as an external forcing which can be also viewed as a control input:

$$\Psi_t = \partial_x\Big\{T_0 \exp[-\beta J * \Psi]\Big(\partial_x\Psi - \beta\Psi(1-\Psi)\partial_x\Big(J * \Psi - \frac{2}{\beta}H\Big)\Big)\Big\}. \tag{4.15}$$

Substituting (4.15) in (4.14) follows that

$$L(\Psi, \Psi_t) = \langle H_x, T_0\Psi(1-\Psi)\exp[-\beta\overline{U}\,]H_x\rangle_{L^2}.$$

Hence the rate function in the limit is

$$S(\Psi) = \int_0^T\int_0^1 T_0\Psi(1-\Psi)\exp[-\beta\overline{U}\,](H_x)^2 \mathrm{d}x\,\mathrm{d}t, \tag{4.16}$$

where H satisfies (4.15). The rate function in (4.16) is identical to the rate function defined in [4, p. 1077], where the authors derived a large deviation principle from the hydrodynamic limit of the microscopic system in Subsection 2.1 with long-range, mean-field type interactions for Kawasaki dynamics.

This asymptotic equivalence of the action functional shows that two processes have the same asymptotic invariant measure. The same asymptotic equivalence of the rate functions implies that the two processes have similar dynamical properties and have the same probability of rare events and exit times. This was shown in [6] where the author derived an action functional and studied nucleation, exit times using the large deviation techniques for the mean field Ising model. A similar analysis of the dynamical properties in finite dimensions is present in [8].

4.3 Mesoscopic simulation of Ostwald ripening using spectral methods

In [15], the author studied the long time behavior of microscopic diffusion dynamics with interactions, such as Ostwald ripening, bypassing the computationally intractable MC simulations and instead using the SPDE approximation (4.3). In [15] spectral methods are used to simulate (4.3), which are based on a spectral representation of the multiplicative noise term. Using the Fourier series representation, the noise term in (4.3) is calculated by completing all multiplications in physical space and all differentiations in Fourier space, passing back and forth between physical space and Fourier space as necessary using the Fast Fourier Transform. Hence this allows to write the solution of (4.3) effectively as a solution of a system of SDE's of the following form

$$u_t = a(u)\mathrm{d}t + b(u)\mathrm{d}W(t). \tag{4.17}$$

Using the LDP perspective presented in Subsection 4.2, it is expected that we can derive the action functional (4.16) in order to demonstrate that the SDE approximation in (4.17) accurately reproduces the long time behavior of the microscopic Monte-Carlo diffusion.

5 Numerical Results

In this section we study the accuracy of the CGL model through numerical experiments. We compare the results from various CGL simulations to those of CGMC simulations, microscopic KMC simulations and continuum mesoscopic equations derived in Section 4. The first set of simulations are simulations with Dirichlet boundary conditions, followed by simulations with periodic boundary conditions.

5.1 Dirichlet boundary conditions

In the simulations with Dirichlet boundary conditions, we use a piecewise constant potential with an interaction radius L given by

$$\begin{aligned} J(x-y) &= \frac{1}{2L}V\Big(\frac{N(x-y)}{L}\Big), \\ V(r) &= \begin{cases} J_0, & |r| \le 1, \\ 0, & |r| > 1, \end{cases} \end{aligned} \tag{5.1}$$

where J_0 is a parameter, the sign of this parameter describes attractive ($J_0 > 0$) or repulsive ($J_0 < 0$) interactions. In these simulations, Dirichlet boundary conditions of 1 and 0 are set at the two boundary nodes and these values extend to the distance L outside the domain regarding the calculation of the energy of particles in cells located near the boundaries (within distance L). Physically these simulations model permeation through a micro porous membrane. These simulations are similar to those presented in [23, 31] and are compared to continuum deterministic mesoscopic equations, i.e., (4.1) without the noise term, and also CGMC simulations.

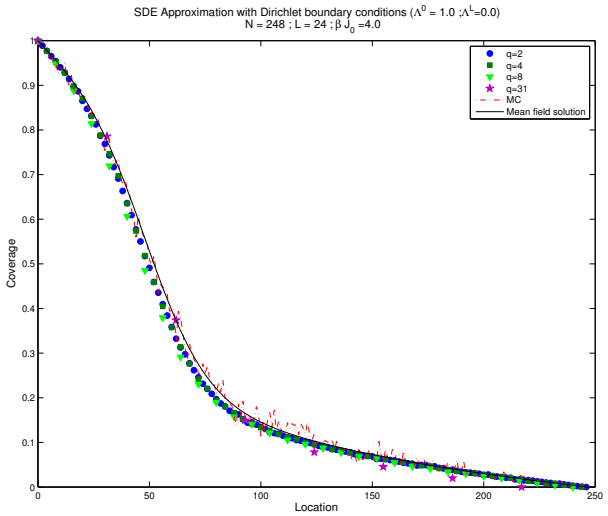

Figure 1 Coverage profiles from CGL with boundary conditions of 1.0 and 0 for various values of q indicated with $\beta J_0 = 4.0$. Also shown are the coverage profiles from microscopic process (MC) and mean field solution. Excellent agreement is observed for the lower values of q.

Long-range interactions Figure 1 shows the coverage profiles on a lattice of size $N = 248$ and a piecewise potential with an interaction radius $L = 24$. The simulations are performed

under the boundary conditions of 1.0 and 0.0, for different coarse-graining levels q and $\beta J_0 = 4.0$. The value of $\beta J_0 = 4.0$ corresponds to the critical point of the 1-D Ising model. We observe good agreement of the CGL model predictions with both the Microscopic process and the mean field solution. In Figure 2 we show the results for simulations at lower temperatures such that $\beta J_0 = 6.0$ and with the other parameters the same as in Figure 1, noting that this value of $\beta J_0 = 6.0$ corresponds to the phase transition regime. The comparison of the CGL model predictions with both the Microscopic process and the mean field solution shows excellent agreement.

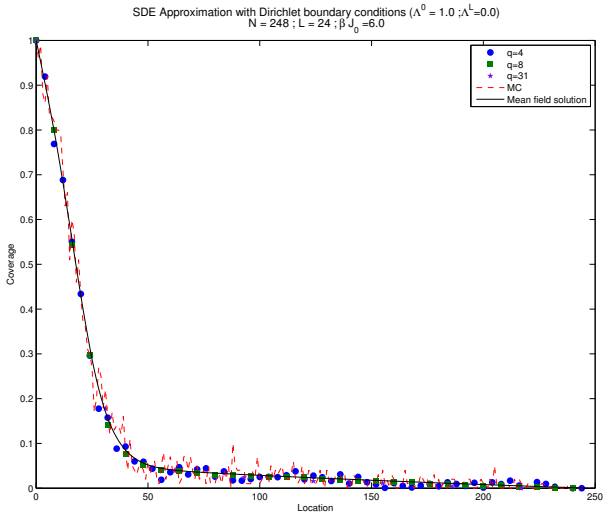

Figure 2 Coverage profiles from CGL with boundary conditions of 1.0 and 0 for various values of q indicated with $\beta J_0 = 6.0$ along with the coverage profiles from microscopic process (MC) and mean field solution. Excellent agreement is observed for the lower values of q.

Short-range interactions Figure 3 shows the coverage profiles on the lattice of size $N = 248$ with short range interactions $L = 6$ and with the boundary conditions of 1.0 and 0.0, $\beta J_0 = 6.0$ and $q = 1$ for CGMC, CGL and the mesoscopic solution. The solution of the CGL seems to agree with the mean field equation but not with CGMC. The reason for such a big difference between CGMC and CGL is that, when $q = 1$, the error term (3.8) in Section 3 is big. The reason why CGL follows the mean field equation is evident from the discussion in Section 4.

Morse potentials In the next set of simulations we use a Morse potential, which is given by

$$V(x) = -A\Big[-2\exp\Big[\frac{x_0 - x}{b}\Big] + \exp\Big[\frac{2(x_0 - x)}{b}\Big]\Big], \quad x \geq 0,$$

where A is the energy at $x = x_0$, x_0 determines the distance to the minimum of the potential and b is the curvature at x_0 that controls the rate of decay of the potential with distance toward zero, i.e., the range of interactions. Figure 4 shows the coverage profiles on a lattice of size $N = 248$ with three different sets of parameters for the Morse potential. In the first case when $x_0 = 1.0$ and $b = 1.0$, the interactions are short ranged interactions with both repulsive and attractive interactions. In the second case when $x_0 = 4.0$ and $b = 1.0$, the interactions are

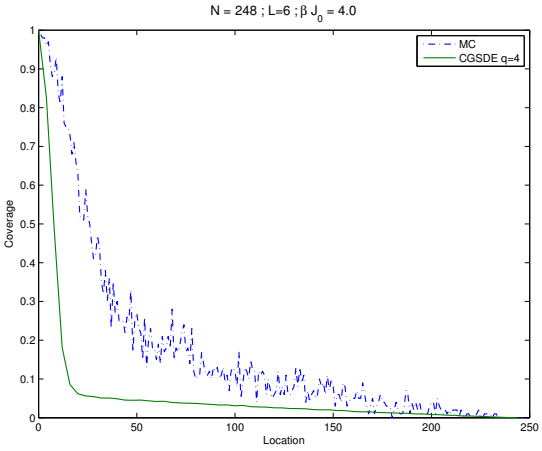

Figure 3 Coverage profiles from CGMC, CGL and mean field with $\beta J_0 = 6.0$ for an interaction radius of $L = 6$. The blue dotted line represents the microscopic process (MC) and the green line represents the CGL with $q = 4$.

long ranged but again with both repulsive (short range) and attractive interactions. In the case when $x_0 = 1.0$ and $b = 5.0$, the interactions are attractive and long ranged. In the simulations with different values of x_0 and b, we choose A such that the zeroth moment is the same in all the cases. The results from these three kinds of potentials again agree with the observations made in the case with piecewise constant potential and the error estimates presented in (3.8), namely that the CGL seems to perform better when the interactions are long ranged. Note that when $x_0 = 1.0$ and $b = 5.0$, the interactions are very weak and almost Fickian.

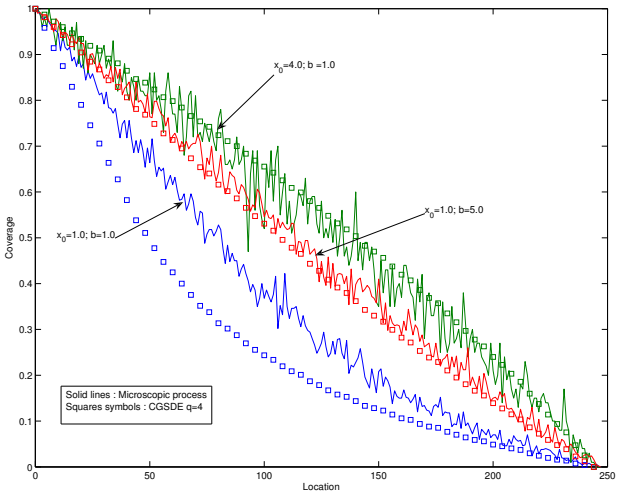

Figure 4 Coverage profiles comparing CGL with the microscopic process. The solid lines represent the coverage profiles from the microscopic process, the square symbols represent the CGL with $q = 4$.

5.2 Periodic boundary conditions

The results from the simulations under an overall gradient suggest that maybe the noise

does not play an important role. To understand how well the noise is captured by the Langevin approximations, we perform the numerical experiments with periodic boundary conditions.

Time scaling In these simulations we use a lattice of size $N = 400$ and a piecewise constant potential as in (5.1) with interaction radius of $L = 40$. In Figure 5 we compare the profiles from CGMC and CGL for $q = 10$. In Figure 6 we compare the Hamiltonian per site versus dimensionless time for CGMC and CGL for the three levels of coarse-graining indicated. Figure 7 shows the Hamiltonian per site versus dimensionless scaled time, tq^2 for three values of q indicated. There is good agreement for the different levels of coarse graining. This also supports the time scaling, first suggested in [23]: due to the coarse graining each spin exchange between two coarse cells requires approximately q^2 jumps. The agreement of the coarse Hamiltonian at different coarse levels also suggests that the Langevin approximation is also capturing effectively the spatial correlations that are included in the Hamiltonian.

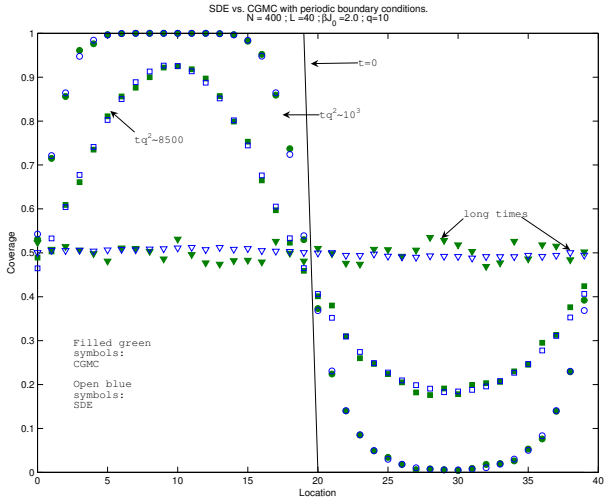

Figure 5 Comparison of coverage profiles from CGMC and SDE's with periodic boundary conditions.

Auto correlation and power spectra comparison The idea of these simulations is to study the long time behavior of the Langevin approximation considered in this paper; to this effect we look at statistical quantities like auto correlations and power spectra. In Figure 8 we plot the auto correlation function of the coverage at a coarse location on the coarse lattice for CGMC and CGL for $q = 10$. The agreement between the auto correlation function shows us that the noise is being correctly represented by the CGL. In fact this is not surprising, as we observed the same behavior in the case of spin-flip dynamics (see Figure 14).

A comparison spatial power spectrum of the coverage profiles gives an idea as to how well the noise is being modeled. In Figure 10 we compare the power spectra of CGMC and CGL for different interaction potential radii L and fixed $q = 20$ for the same long time T. Figure 11 shows agreement at all frequencies between the power spectra for the case $L = 80$. It is observed that agreement between the power spectra is better as $\frac{q}{L}$ decreases. This is shown in Figure 12, where we compare the power spectra for the microscopic case and CGL with $q = 4$ with $N = 4000$, $L = 80$ and $\beta J_0 = 5.0$. Note that for this comparison to be consistent (with

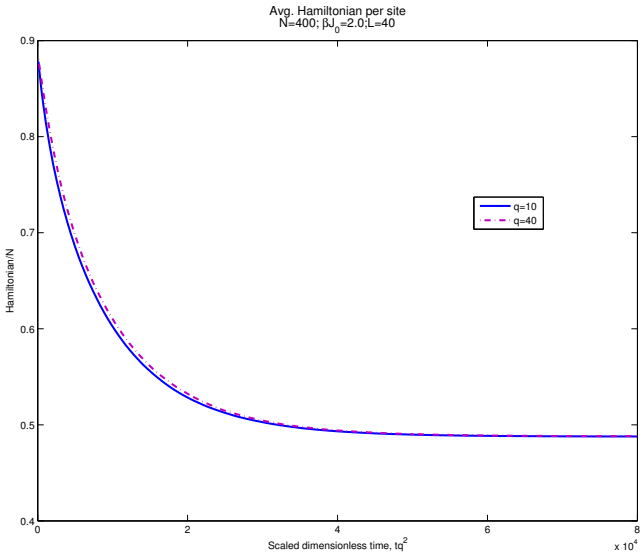

Figure 6 Spatial average Hamiltonian per site vs scaled time, tq^2.

Figures 10 and 11) we average the coverage profile over 20 cells and we observe good agreement between the power spectra of the two processes.

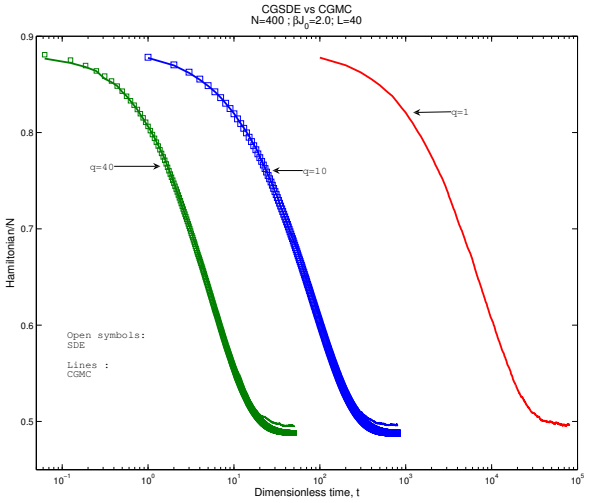

Figure 7 Spatial average Hamiltonian per site vs time, t.

Lifshitz-Slyosov growth law Another important simulation that validates both the model and the numerical scheme is to test if the Lifshitz-Slyosov growth law (see [27]) holds. This law states that the typical length scale in such a conservative nucleating system grows like t^n, where $n = \frac{1}{3}$ at intermediate times, i.e.,

$$R \sim t^{\frac{1}{3}}.$$

In order to measure the typical length scale, we need to look at statistical quantities such as the auto correlation (in space) on the lattice and the spectral density of the coverage profiles

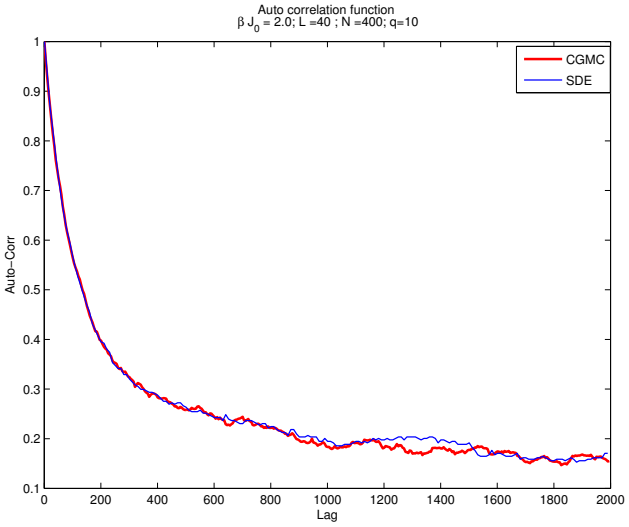

Figure 8 Auto-correlation function of coverage at a coarse location for CGMC and SDE.

(see [16, 28]). The autocorrelation function is defined as

$$G(k,t) = \frac{1}{N^2}\sum_{i\in\mathcal{L}} \eta(i)\eta(i+k) - \langle\eta\rangle^2,$$

where $\langle\eta\rangle$ is the mean coverage at the lattice, which here is constant due to the conservation of mass. One way to determine the typical length scale is to look at the Fourier transform of the autocorrelation which is the spectral density function

$$S(\xi,t) = \widehat{G}(\xi,t).$$

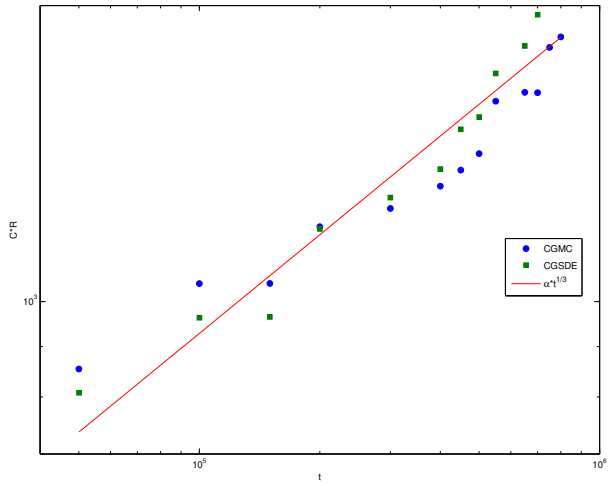

Figure 9 Log-log plot of the mean value proportional to the domain scale versus time for CGMC and CGL. The red solid line has slope $\frac{1}{3}$, the blue circles represent CGMC and the blue square symbols represent CGL. The scaling is evident in both cases.

The first moment or the mean of the spectral density function is inversely proportional to the

typical length scale of the system

$$\overline{\xi}(t) = \frac{\sum\limits_{\xi} \xi S(\xi, t)}{\sum\limits_{\xi} S(\xi, t)}.$$

In Figure 9 we show the scaling for CGL and CGMC with $\beta J_0 = 6.0$. The reader should bear in mind that because of the high coarse graining we cannot capture the scales at the initial times as they are absorbed by the coarse-graining and the coarse-graining also explains the spread of the data. Hence if one were to run the same test with lower coarse-graining we would expect much better agreement.

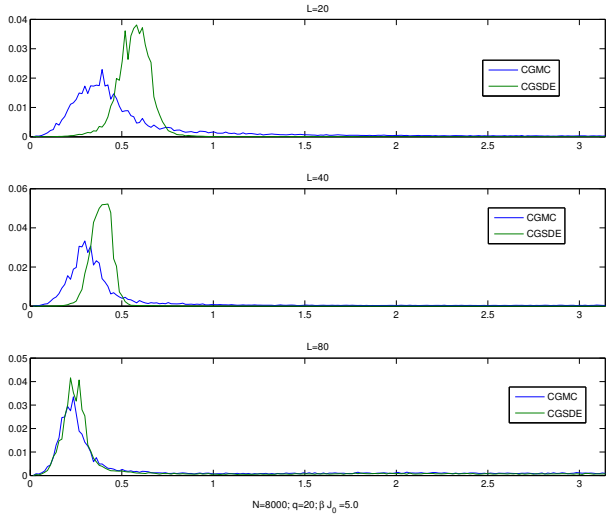

Figure 10 Plot comparing power spectra for CGMC and CGL for three different interaction radii $L = 20, 40, 60$ for $q = 20$. The agreement between the power spectra gets better as $\frac{q}{L}$ is decreases.

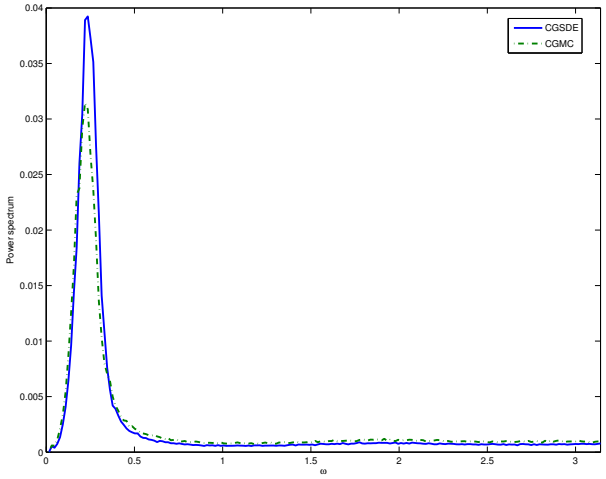

Figure 11 Plot comparing power spectra for CGMC and CGL for $N = 8000$, $L = 80$, $\beta J_0 = 5.0$ for $q = 20$. There is good agreement between the power spectra even in the high modes.

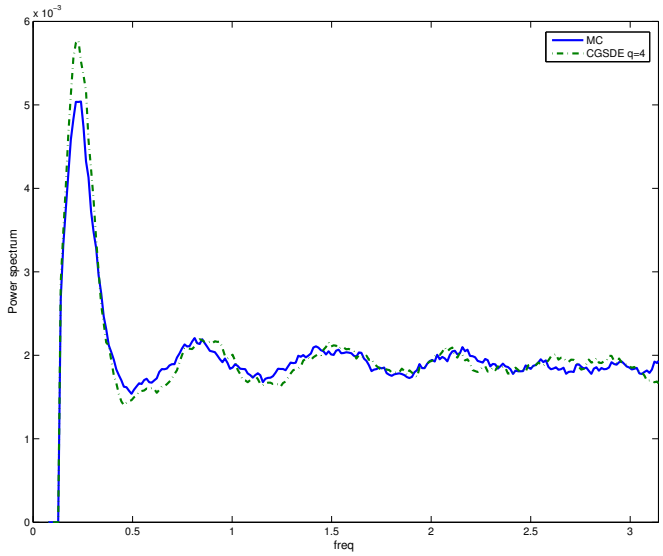

Figure 12 Plot comparing power spectra for CGMC and CGL for $N = 1000$, $L = 80$, $\beta J_0 = 5.0$ for $q = 1$ averaged over 20 microscopic cells. There is good agreement between the power spectra at all modes.

6 Computational Savings and Langevin Dynamics

As shown in [18, 23], coarse-graining of the microscopic process can provide huge computational gains, however the timestep in KMC, both in the microscopic case and the coarse-grained case, depends on the transition probabilities or rates which in turn depend on the interaction potential, the strength of the interactions and the temperature β. The timestep in the Langevin approximation of the MC simulations is independent of the transition probabilities improving the computational gain achieved by CGMC. We also have to note that in the case of MC, CGMC only one particle is moved at every timestep where as in CGL more than one particle can be moved in one timestep. Table 1 shows the CPU times for MC (microscopic), CGMC and CGL with periodic boundary conditions and piecewise constant potential ($J_0 = 2.0$) for different interaction potential radii and temperatures.

Table 1 Comparison of CPU in seconds for different levels of coarse graining, interaction potential radii and temperatures.

	CGMC/MC				CGL			
	$\beta J_0 < 4.0$		$\beta J_0 > 4.0$		$\beta J_0 < 4.0$		$\beta J_0 > 4.0$	
	$L = 1$	$L = 24$	$L = 1$	$L = 24$	$L = 1$	$L = 24$	$L = 1$	$L = 24$
$q = 1$	576	1290	245	439				
$q = 4$	8.72	13.43	4.18	4.38	0.53	0.94	0.53	0.94
$q = 8$	1.09	1.16	0.50	0.40	0.07	0.1	0.07	0.1

Appendix A

In this appendix we show the detailed calculations used in (4.7) and (4.8). Recall the assumption that $\widetilde{\eta}_t$ in (3.1) approaches a slowly varying profile $\rho(\frac{k}{m}, t)$, in the limit $m \to \infty$.

Using (4.4) we rewrite the drift vector defined in (3.5) as

$$\begin{aligned} a(k) = &\frac{1}{m}\rho_t(x_k)(1-\rho_t(x_k))\partial_x \exp[-\beta(U_0+\overline{U}(k,\rho_t))] + \frac{1}{m}\partial_x\rho_t(x_k)\exp[-\beta(U_0+\overline{U}(k,\rho_t))] \\ &- \frac{1}{m}\rho_t(x_{k-1})(1-\rho_t(x_{k-1}))\partial_x \exp[-\beta(U_0+\overline{U}(k-1,\rho_t))] \\ &- \frac{1}{m}\partial_x\rho_t(x_{k-1})\exp[-\beta(U_0+\overline{U}(k-1,\rho_t))] + O\Big(\frac{1}{m^2}\Big). \end{aligned} \tag{A.1}$$

Substituting (A.1) in the right-hand side of the equation in (4.7), we get

$$\begin{aligned} &\frac{1}{m}\sum_k a_k(\widetilde{\eta})\phi(x_k) \\ &= \frac{1}{m^2}\sum_k \phi(x_k)T_0\{\rho_t(k)(1-\rho_t(k))\partial_x \exp[-\beta\overline{U}(k,\rho_t)] + \partial_x\rho_t(k)\exp[-\beta\overline{U}(k,\rho_t)] \\ &\quad - \rho_t(k-1)(1-\rho_t(k-1))\partial_x \exp[-\beta\overline{U}(k-1,\rho_t)] \\ &\quad - \partial_x\rho_t(k-1)\exp[-\beta\overline{U}(k-1,\rho_t)]\} + O\Big(\frac{1}{m^3}\Big) \quad \text{(using (4.5))} \\ &= \frac{1}{m^3}\sum_{k\in\mathcal{L}_m} T_0\partial_x\phi(x_k)\{\rho_t(k)(1-\rho_t(k))\partial_x \exp[-\beta\overline{U}(k,\rho_t)] \\ &\quad + \partial_x\rho_t(k)\exp[-\beta\overline{U}(k,\rho_t)]\} + O\Big(\frac{1}{m^3}\Big) \\ &= \frac{1}{m^2}\langle T_0[\rho_t(1-\rho_t)\partial_x \exp[-\beta\overline{U}] + \partial_x\rho_t \exp[-\beta(\overline{U}(k,\rho))]], \partial_x\phi\rangle_{l^2} + O\Big(\frac{1}{m^3}\Big) \\ &= \frac{1}{m^2}\langle \partial_x T_0[\rho_t(1-\rho_t)\partial_x \exp[-\beta\overline{U}] + \partial_x\rho_t \exp[-\beta\overline{U}]], \phi\rangle_{l^2} + O\Big(\frac{1}{m^3}\Big), \end{aligned}$$

where $T_0 = \exp[-\beta U_0]$, $\overline{U}(k,\rho) = \sum_{\substack{l\in\mathcal{L}_m \\ l\neq k}} \overline{J}(k,l)\rho(l) + \overline{J}(0,0)(\rho(k)-1) - \overline{h}(k)$, and

$$\langle a,b\rangle_{l^2} = \frac{1}{m}\sum_{k\in\mathcal{L}_m} a(k)b(k), \quad \forall\, a,b\in\mathbb{R}^m.$$

Using (4.4), we rewrite that diffusion coefficients defined in (3.6) as

$$\begin{aligned} D_{k(k+1)} = &\frac{2}{q}\rho_t(x_k)(1-\rho_t(x_k))\exp[-\beta(U_0+\overline{U}(k,\rho_t))] \\ &+ \frac{1}{mq}\partial_x\{\rho_t(x_k)(1-\rho_t(x_k))\exp[-\beta(U_0+\overline{U}(k,\rho_t))]\} + O\Big(\frac{1}{m^2}\Big), \\ D_{k(k-1)} = &\frac{2}{q}\rho_t(x_k)(1-\rho_t(x_k))\exp[-\beta(U_0+\overline{U}(k,\rho_t))] \\ &- \frac{1}{mq}\partial_x\{\rho_t(x_k)(1-\rho_t(x_k))\exp[-\beta(U_0+\overline{U}(k,\rho_t))]\} + O\Big(\frac{1}{m^2}\Big). \end{aligned} \tag{A.2}$$

Also note that

$$D_{kk} = -(D_{k(k-1)} + D_{k(k+1)}). \tag{A.3}$$

By using the relations (A.2) and (A.3) in the right-hand side of the equation in (4.8), the

covariance of the stochastic term in (4.6) evaluated at two different test functions ϕ_1, ϕ_2 is

$$
\begin{aligned}
&\Big\langle \sum_{k\in\mathcal{L}_m}\sum_{j\in\mathcal{L}_m} b^{\mathrm{T}}_{jk}(\rho_t)\phi_1(x_j)\frac{\mathrm{d}B_k}{\mathrm{d}t}, \sum_{l\in\mathcal{L}_m}\sum_{i\in\mathcal{L}_m} b^{\mathrm{T}}_{il}(\rho_t)\phi_2(x_i)\frac{\mathrm{d}B_l}{\mathrm{d}t}\Big\rangle\\
&= \sum_{k,l\in\mathcal{L}_m}\Big\langle \sum_{j\in\mathcal{L}_m} b^{\mathrm{T}}_{jk}(\rho_t)\phi_1(x_j)\frac{\mathrm{d}B_k}{\mathrm{d}t}, \sum_{i\in\mathcal{L}_m} b^{\mathrm{T}}_{il}(\rho_t)\phi_2(x_i)\frac{\mathrm{d}B_l}{\mathrm{d}t}\Big\rangle\\
&= \sum_{k,l\in\mathcal{L}_m}\sum_{j,i\in\mathcal{L}_m}(b^{\mathrm{T}}_{jk}(\rho_t)\phi_1(x_j)\cdot b^{\mathrm{T}}_{il}(\rho_t)\phi_2(x_i))\Big\langle\frac{\mathrm{d}B_k}{\mathrm{d}t},\frac{\mathrm{d}B_l}{\mathrm{d}t}\Big\rangle\\
&= \sum_{k,l\in\mathcal{L}_m}\sum_{j,i\in\mathcal{L}_m}(b^{\mathrm{T}}_{jk}(\rho_t)\phi_1(x_j)\cdot b^{\mathrm{T}}_{il}(\rho_t)\phi_2(x_i))\delta(k-l) = \sum_{j,i\in\mathcal{L}_m}\sum_{k\in\mathcal{L}_m}(b^{\mathrm{T}}_{jk}(\rho_t)\phi_1(x_j)\cdot b^{\mathrm{T}}_{ik}(\rho_t)\phi_2(x_i))\\
&= \sum_{j,i\in\mathcal{L}_m}\sum_{k} b^{\mathrm{T}}_{jk}b_{ki}\phi_1(x_j)\phi_2(x_i) = \sum_{j,i\in\mathcal{L}_m} D_{ij}\phi_1(x_j)\phi_2(x_i) \quad \text{(by definition } D = b^{\mathrm{T}}b)\\
&= \sum_{k\in\mathcal{L}_m}\{D_{k(k-1)}\phi_2(x_{k-1}) + D_{kk}\phi_2(x_k) + D_{k(k+1)}\phi_2(x_{k+1})\}\phi_1(x_k)\\
&= \sum_{k\in\mathcal{L}_m}\{D_{k(k-1)}(\phi_2(x_{k-1})-\phi_2(x_k)) + D_{k(k+1)}(\phi_2(x_{k+1})-\phi_2(x_k))\}\phi_1(x_k) \quad \text{(using (A.3))}\\
&= \sum_{k\in\mathcal{L}_m}\Big\{-\frac{1}{m}D_{k(k-1)}(\partial_x\phi_2(x_k))\phi_1(x_k) + \frac{1}{2m^2}D_{k(k-1)}(\partial_x^2\phi_2(x_k))\phi_1(x_k)\\
&\quad + \frac{1}{m}D_{k(k+1)}(\partial_x\phi_2(x_k))\phi_1(x_k) + \frac{1}{2m^2}D_{k(k+1)}(\partial_x^2\phi_2(x_k))\phi_1(x_k)\Big\} + O\Big(\frac{1}{m^2}\Big)\\
&= \frac{1}{mq}\int\{2T_0\rho(x)(1-\rho(x))\exp[-\beta J*\rho(x)]\}\partial_x\phi_1(x)\partial_x\phi_2(x)\mathrm{d}x + O\Big(\frac{1}{m^2}\Big) \quad \text{(using (A.2))},
\end{aligned}
$$

where $T_0 = \exp[-\beta U_0]$ and $\overline{U}(k,\rho) = \sum_{\substack{l\in\mathcal{L}_m\\ l\neq k}} \overline{J}(k,l)\rho(l) + \overline{J}(0,0)(\rho(k)-1) - \overline{h}(k)$. Now the covariance of the stochastic term in (4.1) evaluated at two different test function ϕ_1, ϕ_2 is

$$
\begin{aligned}
&\Big\langle \int \frac{1}{\sqrt{mq}}\partial_x\{[2T_0\exp[-\beta J*\rho]\rho(1-\rho)]^{\frac{1}{2}}\dot{W}\}\phi_1(x)\mathrm{d}x,\\
&\quad \int \frac{1}{\sqrt{mq}}\partial_x\{[2T_0\exp[-\beta J*\rho]\rho(1-\rho)]^{\frac{1}{2}}\dot{W}\}\phi_2(y)\mathrm{d}y\Big\rangle\\
&= \frac{1}{mq}\Big\langle \int\{[2T_0\exp[-\beta J*\rho(x)]\rho(x)(1-\rho(x))]^{\frac{1}{2}}\dot{W}(x,t)\}\partial_x\phi_1(x)\mathrm{d}x,\\
&\quad \int\{[2T_0\exp[-\beta J*\rho(y)]\rho(y)(1-\rho(y))]^{\frac{1}{2}}\dot{W}(y,t)\}\partial_x\phi_2(y)\mathrm{d}y\Big\rangle\\
&= \frac{2T_0}{mq}\iint\{\exp[-\beta J*\rho(x)]\rho(x)(1-\rho(x))\}^{\frac{1}{2}}\partial_x\phi_1(x)\\
&\quad \cdot\{\exp[-\beta J*\rho(y)]\rho(y)(1-\rho(y))\}^{\frac{1}{2}}\partial_x\phi_2(y)\langle\dot{W}(x,t),\dot{W}(y,t)\rangle\mathrm{d}x\,\mathrm{d}y\\
&= \frac{2T_0}{mq}\iint\{\exp[-\beta J*\rho(x)]\rho(x)(1-\rho(x))\}^{\frac{1}{2}}\partial_x\phi_1(x)\\
&\quad \cdot\{\exp[-\beta J*\rho(y)]\rho(y)(1-\rho(y))\}^{\frac{1}{2}}\partial_x\phi_2(y)\delta(x-y)\mathrm{d}x\,\mathrm{d}y\\
&= \frac{1}{mq}\int\{2T_0\rho(x)(1-\rho(x))\exp[-\beta J*\rho(x)]\}\partial_x\phi_1(x)\partial_x\phi_2(x)\mathrm{d}x,
\end{aligned}
$$

where $T_0 = \exp[-\beta U_0]$.

Appendix B

In this appendix we show the calculations involved in the calculation of CGL parameters in the presence of boundary conditions. Boundary conditions define the rates at the two boundary cells which in turn determine the coefficients of the drift vector (3.5) and diffusion matrix (3.7). The two boundary conditions we are interested in are

Dirichlet Boundary conditions In this case Dirichlet boundary conditions of 1 and 0 are set at the boundary nodes side and also flux out of the lattice at the boundaries is set to zero. When we apply a boundary condition of 1 to the first cell on the lattice the rate $\overline{c}(2 \mapsto 1, \widetilde{\eta}) = 0$. Similarly, when we apply boundary condition of 0 to last cell, the rate $\overline{c}(m \mapsto m-1, \widetilde{\eta}) = 0$. The drift terms and the diffusion coefficients at the boundaries are given by

$$\begin{aligned}
a(1) &= -\frac{1}{q}c(1 \mapsto 2, \eta), & a(m) &= \frac{1}{q}c(m-1 \mapsto m, \eta),\\
D_{11} &= \frac{1}{q^2}\overline{c}(1 \mapsto 2, \eta), & D_{12} &= -\frac{1}{q^2}\overline{c}(1 \mapsto 2, \eta),\\
D_{mm} &= \frac{1}{q^2}\overline{c}(m-1 \mapsto m, \eta), & D_{m(m-1)} &= -\frac{1}{q^2}\overline{c}(m-1 \mapsto m, \eta).
\end{aligned}$$

Periodic Boundary conditions In the case when we have periodic boundary conditions, there is flux between the two boundary nodes as there is interaction between the two nodes. The drift terms and the diffusion coefficients at the boundaries are given by

$$\begin{aligned}
a(1) &= \frac{1}{q}(c(m \mapsto 1, \eta) + c(1 \mapsto 2, \eta) - c(1 \mapsto m, \eta) - c(1 \mapsto 2, \eta)),\\
a(m) &= \frac{1}{q}(c(m \mapsto m-1, \eta) + c(m \mapsto 1, \eta) - c(1 \mapsto m, \eta) - c(m-1 \mapsto 1, \eta)),\\
D_{11} &= \frac{1}{q^2}(\overline{c}(1 \mapsto 2, \eta) + \overline{c}(2 \mapsto 1, \eta) + \overline{c}(m \mapsto 1, \eta) + \overline{c}(1 \mapsto m, \eta)),\\
D_{12} &= -\frac{1}{q^2}(\overline{c}(1 \mapsto 2, \eta) + \overline{c}(2 \mapsto 1, \eta)),\\
D_{mm} &= \frac{1}{q^2}(\overline{c}(m \mapsto m-1, \eta) + \overline{c}(m-1 \mapsto m, \eta) + \overline{c}(m \mapsto 1, \eta) + \overline{c}(1 \mapsto m, \eta)),\\
D_{m(m-1)} &= -\frac{1}{q^2}(\overline{c}(m \mapsto m-1, \eta) + \overline{c}(m-1 \mapsto m, \eta)).
\end{aligned}$$

Accordingly, the matrix b is given by

$$\begin{aligned}
b_{m1} &= \frac{1}{q}\sqrt{\overline{c}(1 \mapsto m, \eta) + \overline{c}(m \mapsto 1, \eta)}\,,\\
b_{kk} &= \frac{1}{q}\sqrt{\overline{c}(k \mapsto k+1, \eta) + \overline{c}(k+1 \mapsto k, \eta)}\,,\\
b_{(k+1)k} &= -b_{kk},\\
b_{ij} &= 0, \quad \text{otherwise.}
\end{aligned}$$

Remark The spin exchange dynamics are conservative, i.e., the total spin on the lattice is always conserved in the case with periodic boundary conditions. The stochastic approximation presented above with periodic boundary conditions satisfy this very basic requirement and this can easily be checked $\left(\text{i.e., } \sum_k \mathrm{d}\widetilde{\eta}_k = 0\right)$. The criteria of conservation is not seen in the the case with Dirichlet boundary conditions as the flux across the boundary is not balanced.

Appendix C Langevin Approximation of Non-conservative Dynamics

In this appendix, we recall the Langevin approximation of spin flip dynamics presented in [21] and compare the long time behavior of the Langevin approximation for spin flip dynamics to long time behavior of the Langevin approximation of diffusion mechanisms in Section 3.

Microscopic model The microscopic stochastic model for the spin flip mechanism is defined on a periodic lattice of size N which we denote by $\mathcal{L}_N = \{1, 2, \cdots, N\}$. At each lattice site $x \in \mathcal{L}_N$ is an associated spin taking values 0 or 1. A spin configuration σ is an element of the configuration space $\Sigma = \{0,1\}^{\mathcal{L}_N}$. The resulting stochastic process $\{\sigma_t\}_{t\geq 0}$ is a continuous time jump Markov process on $L^\infty(\Sigma;\mathbb{R})$ with generator (see [24])

$$Lf(\sigma) = \sum_{x\in\mathcal{L}_N} c(x,\sigma)(f(\sigma^x) - f(\sigma)) \tag{C.1}$$

for any test function $f \in L^\infty(\Sigma;\mathbb{R})$. Here $c(x,\sigma)$ denotes the rate of the process and σ^x signifies the configuration after a flip at x. The Arrhenius rate is defined as

$$c(x,\sigma) = c_a(1-\sigma(x)) + c_d\sigma(x)\mathrm{e}^{-\beta U(x,\sigma)}, \tag{C.2}$$

where $U(x,\sigma)$ is the potential which is given by (2.3). It can be easily verified that the Arrhenius rate defined in (C.2) satisfies detailed balance.

Coarse grained model The coarse-grained model is similar to the coarse-graining presented earlier in Subsection 2.2. Using the same setup as in Subsection 2.2 and rewriting the generator in (C.1), we have the following generator for $\{\eta_t\}$ (see [18]):

$$\overline{\mathcal{L}}^c g(\eta) = E\sum_{k\in\mathcal{L}_m} c_a(k)(g(\eta+\delta_k) - g(\eta)) + c_d(k)(g(\eta-\delta_k) - g(\eta)),$$

where $g \in L^\infty(\mathcal{H}_{mq};\mathbb{R})$ is a test function, $c_a(k)$ and $c_d(k)$ are the coarse grained adsorption and desorption rates

$$c_a(k,\eta) = d_0(q-\eta(k)), \quad c_d(k,\eta) = d_0\eta(k)\mathrm{e}^{-\beta\overline{U}(k,\eta)},$$

where the new interaction potential $\overline{U}(k,\eta)$ represents an approximation of the original interaction potential $U(x,\sigma)$ and is given by (2.3).

We present this SDE approximation of spin-flip mechanisms presented in [21] using the Curie-Weiss model as an example. In the Curie-Weiss case the microscopic spin flip dynamics coarse grain exactly: since the interaction potential is uniform and constant, the error due to coarse graining is zero. This is described in more detail in [17] where the coarse grained process described in [17, pp. 256–259] is exact. We choose the Curie-Weiss case because it can be coarse grained exactly hence isolating the error from the SDE approximation.

Coarse grained Curie-Weiss model The Curie-Weiss model is a Ising model defined on a lattice $\mathcal{L}$ of N lattice sites. At each site of the lattice we have a spine $\sigma(x) \in \{-1,1\}$. The interaction potential is constant and every site interacts with every other site of the lattice. The potential is given by

$$J(x-y) = \frac{J_0}{N}, \quad x,y \in \mathcal{L}.$$

The microscopic Hamiltonian in (2.1) can be written exactly in terms of the coarse variable $\eta := \frac{1}{N}\sum_{x\in\mathcal{L}}\sigma(x)$ as the coarse grained Hamiltonian

$$H(\sigma) = \overline{H}(\eta) := N\widetilde{H}(\eta) = N\Big(-\frac{J_0}{2}\eta\Big(\eta - \frac{1}{N}\Big) + h\eta\Big).$$

Since coarse-graining is exact, the coarse-grained invariant measure is obtained from the microscopic Gibbs measure, $\exp[-\beta H(\sigma)] = \exp[-\beta\overline{H}(\eta)]$,

$$\mu(\eta) = \frac{1}{Z}\exp[-\beta\overline{H}(\eta)]P_N(\eta),$$

where the product binomial distribution

$$P_N\Big(\eta = \frac{k}{N}\Big) = \frac{N!}{k!(N-k)!}\Big(\frac{1}{2}\Big)^N$$

is the prior distribution arising from the microscopic prior by including N independent sites (see [1]). The above Gibbs measure, using Stirling's formula, can be written as

$$\begin{aligned}\mu_0\Big(\eta = \frac{k}{N}\Big) &= Z^{-1}\mathrm{e}^{\beta\overline{H}(\eta)+\log(N!)-\log(k!)-\log((N-k)!)-N\log(2)}\\ &= Z^{-1}\mathrm{e}^{-N(\beta\widetilde{H}(\eta)+\eta\log(\eta)+(1-\eta)\log(1-\eta)+O(N^{-1}))}\\ &=: Z^{-1}\mathrm{e}^{-N\beta U(\eta)},\end{aligned} \tag{C.3}$$

where $U(\eta) := \beta\widetilde{H}(\eta) + \eta\log(\eta) + (1-\eta)\log(1-\eta)$.

Langevin approximation of Curie-Weiss model The SDE approximation for the above defined coarse grained Markov process $\{\widetilde{\eta}_t\}$ is given by (see [21])

$$\mathrm{d}\widetilde{\eta} = a(\widetilde{\eta})\mathrm{d}t + b(\widetilde{\eta})\mathrm{d}W_t, \tag{C.4}$$

where

$$\begin{aligned}a(x) &= 1 - x - x\exp\Big[-\beta\Big(J\Big(x - \frac{1}{N}\Big) - h\Big)\Big],\\ b(x) &= \sqrt{\frac{|1 - x + x\exp[-\beta(J(x-\frac{1}{N}) - h)]|}{N}}.\end{aligned}$$

The density of the invariant measure of the 1-D stochastic differential equation is (see [3, Section 5.2.2])

$$\nu(\widetilde{\eta}) = \frac{1}{\widetilde{Z}}\exp\Big[2\int_0^{\widetilde{\eta}}\frac{a(x)}{b^2(x)}\mathrm{d}x - \log b^2(\widetilde{\eta})\Big]$$

or

$$\nu(\widetilde{\eta}) = \frac{1}{\widetilde{Z}}\exp[-NV(\widetilde{\eta})],$$

where

$$\begin{aligned}V(\widetilde{\eta}) = &-2\int_0^{\widetilde{\eta}}\frac{1 - x - x\exp[-\beta(J(x-\frac{1}{N}) - h)]}{1 - x + x\exp[-\beta(J(x-\frac{1}{N}) - h)]}\mathrm{d}x\\ &+\frac{1}{N}\log\Big(1 - \widetilde{\eta} + \widetilde{\eta}\exp\Big[-\beta\Big(J\Big(\widetilde{\eta} - \frac{1}{N}\Big) - h\Big)\Big]\Big).\end{aligned}$$

It can easily be shown that the asymptotically the two measures $\nu(\widetilde{\eta})$ and $\mu(\eta)$ are equivalent by noticing that the functions U and V have the same critical points upto the order of $O(N^{-1})$. But this asymptotic equivalence is not sufficient to approximate all expected values, for example exit times (see [12, 13, 21]).

As a remedy for this, a different SDE approximation of the master equation with the same asymptotic drift but a modified diffusion (referred to as "Hanggi-diffusion" in [21]) based on the invariant distribution of CGMC was proposed in [12]. The new SDE for $\{\overline{\eta}_t\}$ is given by

$$\mathrm{d}\overline{\eta} = \Big(a(\overline{\eta}) + \frac{1}{N}c(\overline{\eta})\Big)\mathrm{d}t + \frac{1}{\sqrt{N}}\overline{b}(\overline{\eta})\mathrm{d}W_t, \tag{C.5}$$

where

$$a(x) = 1 - x - x\exp\Big[-\beta\Big(J\Big(x - \frac{1}{N}\Big) - h\Big)\Big]$$

and

$$c(x) = \Big(-\frac{a(x)}{U'(x)}\Big)', \quad \overline{b}(x) = \sqrt{-\frac{2a(x)}{U'(x)}}.$$

It can be shown that the above SDE has the same invariant distribution as the coarse grained dynamics. The invariant distribution μ is given by (C.3).

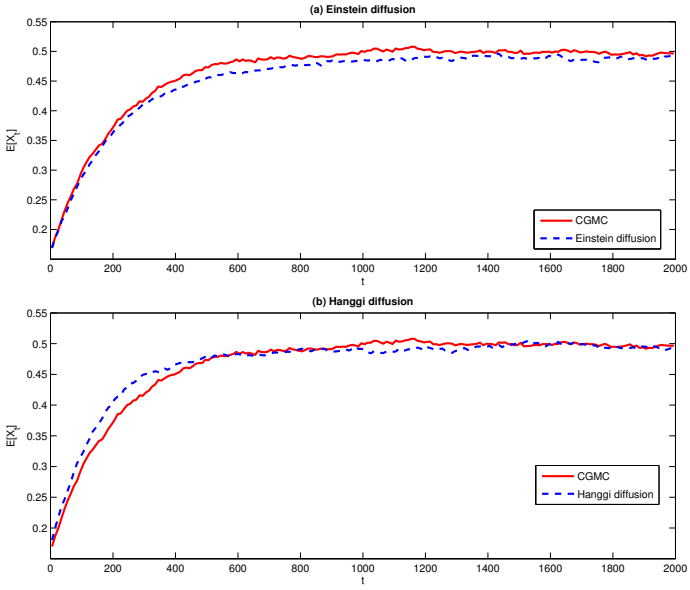

Figure 13 Comparison of the mean path of the two stochastic processes with CGMC simulations.

In Figure 13 we compare the mean paths of the Langevin approximation (C.4) and the SDE approximation using Hanggi-diffusion (C.5) to the exact coarse-grained process with $N = 100$, $\beta = 2.50$, $J_0 = 2.0$. It can be seen that even though the Langevin process agrees well with the coarse-grained process for smaller times, it drifts away as the time gets bigger which is because of the different invariant measures. In the case of Hanggi-diffusion, the short time behavior is not good but the long time behavior is in agreement with CGMC: in Figure 14 we

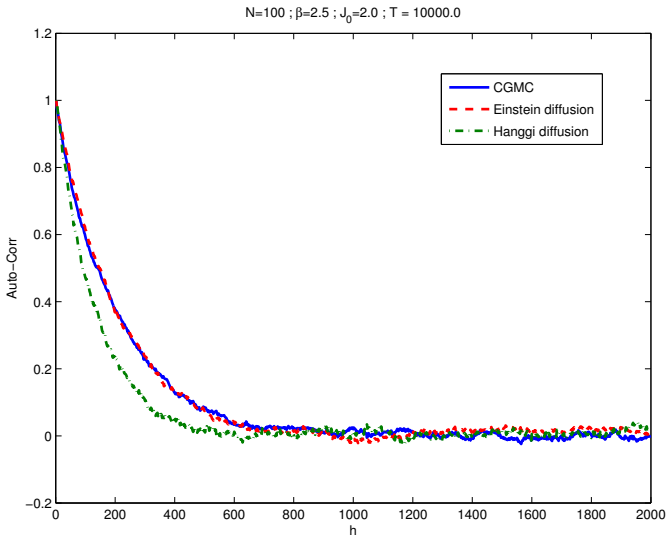

Figure 14 Comparison of the auto correlation function of the Langevin approximation and Hanggi-diffusion with auto correlation function of CGMC simulation.

compare the correlation function for the two Langevin approximations and compare them with the correlation function for the CGMC simulations. Overall, the Langevin approximation has better short time behavior, while at long time the SDE approximation with Hanggi-diffusion performs better. Still for observables such as auto-correlations the Langevin approximation is a correct approximation even though it only exhibits good short time behavior. In contrast in Subsection 4.2 we have showed that the Langevin approximation of the diffusion mechanism with interactions asymptotically has always the same long time behavior as the microscopic process.

Acknowledgement The first two authors acknowledge discussions with Professor Luc Rey-Bellet.

References

[1] Abrams, C. F. and Kremer, K., The effect of bond length on the structure of dense bead-spring polymer melts, *J. Chem. Phys.*, **115**, 2001, 2776–2785.

[2] Allen, M. P. and Tildesley, D. J., Computer Simulation of Liquids, Clarendon Press, New York, 1989.

[3] Are, S., Katsoulakis, M. A., Plechac, P., et al, Multi-body interactions in coarse-graining schemes of extended systems, *SIAM Sci. Comput.*, **31**(2), 2008, 987–1015.

[4] Asselah, A. and Giacomin, G., Metastability for the exclusion process with mean-field interaction, *J. Stat. Phys.*, **93**, 1998, 1051–1110.

[5] Chua, A. L.-S., Haselwandter, C. A., Baggio, C., et al, Langevin equations for fluctuating surfaces, *Phys. Rev. E*, **72**, 2005, 051103.

[6] Comets, F., Nucleation for a long range magnetic model, *Ann. Inst. H. Poincaré*, **23**, 1986, 135–178.

[7] Dupuis, P. and Ellis, R. S., A Weak Convergence Approach to the Theory of Large Deviations, John Wiley & Sons, New York, 1997.

[8] Friedlin, M. I. and Wentzell, A. D., Random Perturbations of Dynamical Systems, Second Edition, Springer-Verlag, New York, 1998.

[9] Gardiner, C. W., Handbook of Stochastic Methods, Springer-Verlag, Berlin, 1985.

[10] Giacomin, G. and Lebowitz, J. L., Phase segregration dynamics in particle systems with long range interactions, I, Macroscopic limits, *J. Stat. Phys.*, **87**, 1997, 37–61.

[11] Gillespie, D. T., The chemical Langevin equation, *J. Chem. Phys.*, **113**, 2000, 297–306.

[12] Hanggi, P., Grabert, H., Talkner, P., et al, Bistable systems: master equation versus Fokker-Planck modeling, *Phys. Rev. A*, **3**, 1984, 371–378.

[13] Hanggi, P., Talkner, P. and Borkovec, M., Reaction-rate theory: fifty years after Kramers, *Rev. Mod. Phys.*, **62**, 1990, 251–341.

[14] Hildebrand, M. and Mikhailov, A., Mesoscopic modeling in the kinetic theory of adsorbates, *J. Phys. Chem.*, **100**, 1996, 19089–19101.

[15] Horntrop, D. J., Mesoscopic simulation of Ostwald ripening, *J. Comput. Phys.*, **218**, 2006, 429–441.

[16] Horntrop, D. J., Katsoulakis, M. A. and Vlachos, D. G., Spectral methods for mesoscopic models for pattern formation, *J. Comput. Phys.*, **173**, 2001, 364–390.

[17] Katsoulakis, M. A., Majda, A. J. and Sopasakis, A., Multiscale couplings in prototype hybrid deterministic /stochastic systems, I, Deterministic closures, *Commun. Math. Sci.*, **2**, 2004, 255–294.

[18] Katsoulakis, M. A., Majda, A. J. and Vlachos, D. G., Coarse-grained stochastic processes and Monte Carlo simulations in lattice systems, *J. Comput. Phys.*, **186**, 2003, 250–278.

[19] Katsoulakis, M. A., Plecháč, P. and Sopasakis, A., Error analysis of coarse-graining for stochastic lattice dynamics, *SIAM J. Numer. Anal.*, **44**, 2006, 2270–2296.

[20] Katsoulakis, M. A., Rey-Bellet, L., Plecháč, P., et al, Coarse-graining schemes and a posteriori error estimates for stochastic lattice systems, *Math. Modelling Numer. Anal.*, **41**, 2006, 327–660.

[21] Katsoulakis, M. A. and Szepessy, A., Stochastic hydrodynamical limits of particle systems, *Commun. Math. Sci.*, **4**, 2006, 513–549.

[22] Katsoulakis, M. A. and Trashorras, J., Information loss in coarse-graining of stochastic particle dynamics, *J. Stat. Phys.*, **122**, 2006, 115–135.

[23] Katsoulakis, M. A. and Vlachos, D. G., Coarse-grained stochastic processes and kinetic Monte Carlo simulators for the diffusion of interacting particles, *J. Chem. Phys.*, **119**, 2003, 9412–9427.

[24] Kipnis, C. and Landim, C., Scaling Limits of Interacting Particle Systems, Springer-Verlag, New York, 1999.

[25] Kipnis, C., Olla, S. and Varadhan, S., Hydrodynamic and large deviations for simple exclusion process, *Comm. Pure Appl. Math.*, **42**, 1989, 115–137.

[26] Landau, D. P. and Binder, K., A Guide to Monte Carlo Simulations in Statistical Physics, Cambridge University Press, Cambridge, 2000.

[27] Lifshitz, I. and Slyozov, V., The kinetics of precipitaton from supersaturated solid solutions, *J. Phys. Chem. Solids*, **19**, 1961, 35–50.

[28] Newman, M. E. J. and Barkema, G. T., Monte Carlo Methods in Statistical Physics, Oxford University Press, Oxford, 1999.

[29] Pivkin, I. and Karniadakis, G., Coarse-graining limits in open and wall-bounded dissipative particle dynamics systems, *J. Chem. Phys.*, **124**, 2006, 184101.

[30] Sopasakis, A. and Katsoulakis, M. A., Stochastic modeling and simulation of traffic flow: asymmetric single exclusion process with Arrhenius look-ahead dynamics, *SIAM J. Appl. Math.*, **66**, 2006, 921–944.

[31] Vlachos, D. G. and Katsoulakis, M. A., Derivation and validation of mesoscopic theories for the diffusion of interacting molecules, *Phys. Rev. Lett.*, **85**, 2000, 3898–3901.

[32] Ziff, R. M., Gulari, E. and Barshad, Y., Kinetic phase transitions in an irreversible surface-reaction model, *Phys. Rev. Lett.*, **56**, 1986, 2553–2556.